Field sampling and field reconstruction: A new perspective

A. Capozzoli,[1] C. Curcio,[1] A. Liseno,[1] and P. Vinetti[1]

Received 25 September 2009; revised 5 June 2010; accepted 2 August 2010; published 16 November 2010.

[1] We address the problem of extracting the maximum amount of information on an electromagnetic field over a domain D_O from field sample measurements on a domain D_I, with a priori information on the source (or scatterer). The problem is faced in two steps. In the first one, the source reconstruction is dealt with by taking into account the available a priori information and the optimal probe positioning is determined as that optimizing the singular value dynamics of the involved linear radiation operator. The second step consists of reconstructing the field on D_O as that radiated by the retrieved source. An extensive numerical analysis highlights the performance of the approach.

Citation: Capozzoli, A., C. Curcio, A. Liseno, and P. Vinetti (2010), Field sampling and field reconstruction: A new perspective, *Radio Sci.*, *45*, RS6004, doi:10.1029/2009RS004298.

1. Introduction

[2] The problem of extracting the maximum amount of information on an electromagnetic field over a domain D_O from field measurements on a domain D_I, with a priori information on the source [*Bertero et al.*, 1979; *Marks*, 1980; *Severcan*, 1982; *Yaghjian*, 1986; *Kao et al.*, 1999; *Schreier et al.*, 2000; *Piestun and Miller*, 2000; *Derat et al.*, 2007; *Vinetti*, 2008; *Gruber and Marengo*, 2008; *Capozzoli et al.*, 2009a] (equivalent current distribution [*Collin*, 1991] or polarization current, contrast source [*Langenberg*, 2002; *Li et al.*, 2009]), henceforth referred to as the source $\underline{J}$, sustaining the radiated (scattered) field of interest, is relevant in a large number of applications.

[3] In optics, for example, a vast amount of literature has been devoted to the problem of object restoration and image extrapolation, in particular, extrapolation outside the pupil from measurements made within the pupil [*Bertero et al.*, 1979; *Marks*, 1980; *Severcan*, 1982]. For this problem, the a priori knowledge usually consists of the finite object's extent and the domain D_O contains D_I. Moreover, much relevance has also the problem of image interpolation, for which the domain D_O is contained in D_I, and the a priori information is employed to mitigate the sampling requirements [*Kao et al.*, 1999] and to improve the accuracy [*Schreier et al.*, 2000].

[4] In microwave and millimeter-wave applications, we mention Near-Field/Far-Field (NFFF) [*Yaghjian*, 1986; *Capozzoli et al.*, 2009a] or Very Near-Field/Far-Field (V-NFFF) [*Vinetti*, 2008] transformations, in which D_I is located within the near-field or very near-field of the radiator to be characterized, while D_O is located in its far-field region and a priori information on the radiator/scatterer geometry is exploited. We also point out applications of electromagnetic compatibility in which D_I and D_O can be disjoint domains located in the near-field region of unintentional sources [*Derat et al.*, 2007]. Finally, we cite Multiple Input Multiple Output systems (MIMO) for which, from receivers located in D_O, it is desired to reconstruct the information transmitted by sources in D_I [*Piestun and Miller*, 2000; *Gruber and Marengo*, 2008].

[5] Typically, collecting the information on D_I is performed by means of field probes, occupying different spatial positions. For this reason, the problem at hand requires determining, as a function of the properties of the employed probes, of the shape and size of the acquisition domain D_I and of the a priori information on the source, the overall number of acquisition points and their optimal spatial distribution to reconstruct "at the best" the required information on D_O [*Cathey et al.*, 1984].

[6] First approaches to the problem of determining the sampling positions on D_I and of subsequently reconstructing (interpolating) the acquired samples within the measurement domain (i.e., $D_O \subseteq D_I$) were proposed, more than four decades ago, in optics [*Toraldo di Francia*, 1955; *Barakat*, 1964], and, later, in tomography [*Fok and Young*, 1987] and antenna measurements [*Rahmat-Samii et al.*, 1980], essentially dealing with the field as a "globally" bandlimited function and straightforwardly applying the Shannon sampling theorem and cardinal interpolation series.

[1]Dipartimento di Ingegneria Biomedica, Elettronica e delle Telecomunicazioni, Università di Napoli Federico II, Naples, Italy.

0048-6604/10/2009RS004298

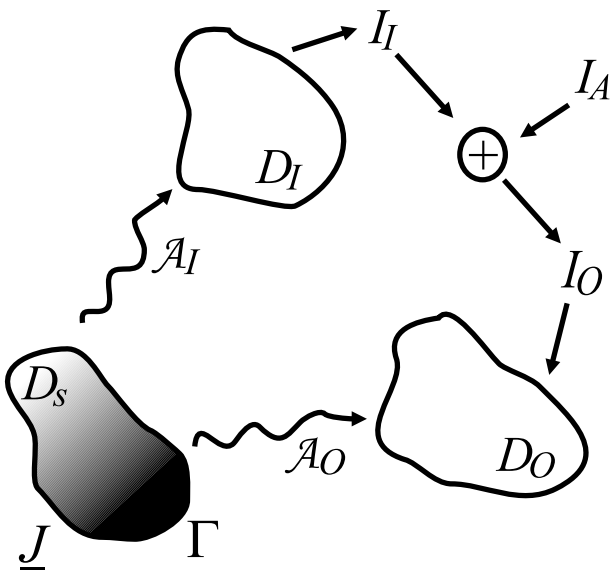

Figure 1. Graph of the problem formulation.

[7] Subsequently, a more efficient method [*Bucci and D'Elia*, 1996; *Bucci et al.*, 1998], based on the concept of "local" bandwidth of the radiated/scattered field, has been developed with the aim of providing a solution to the field sampling and interpolation problem on closed or unlimited, analytical near-field curves. The approach exploits a priori information on the shape and size of the source by assimilating it to an elementary, convex domain (as, for example, a spheroidal volume) containing the source. When applied to finite, open curves, the approach is usually applied by simply truncating the samples lying on a curve of the type above, controlling the truncation error by properly choosing the oversampling and bandwidth enlargement factors [*Bucci and Di Massa*, 1988]. Up to now, this approach has proved successful, allowing a significant improvement if compared to more standard approaches.

[8] It is worth noting that, methods for the sampling and reconstruction (interpolation) problem of bandlimited or nonbandlimited signals and exploiting the concept of "local" bandwidth to reach a nonredundant sampling have been also developed in the field of signal processing [*Clark et al.*, 1985; *Zeevi and Shlomot*, 1993]. In this paper, a more general perspective, based on an operator mathematical formulation, is offered.

[9] More in detail, given a source $\underline{J}$, first the problem of determining the functional subspace containing that part, say $\underline{J}_E$, of $\underline{J}$ which can be estimated from D_I and has image on D_O is afforded as an optimization problem of singular value dynamics [*Curtis*, 2002; *Alonso et al.*, 2004; *Lewis*, 2003]. Then, given the degree of uncertainties, we deal with the problem of extracting the maximum amount of "information" from field samples on D_I about $\underline{J}_E$ to foresee "at the best" the field on D_O. Finally, the determination of the field on D_O is faced in two steps. In the first one, the reconstruction of $\underline{J}_E$ is dealt with by also taking into account the available a priori information. Thanks to the linearity of the mapping between the data (field acquired on D_I) and the unknown ($\underline{J}_E$), the optimal positioning of the probe in D_I is determined, as that optimizing the singular value dynamics of the involved linear operator [*Curtis*, 2002; *Alonso et al.*, 2004; *Lewis*, 2003]. The second step consists of reconstructing the field on D_O as that radiated by the retrievable $\underline{J}_E$.

[10] More in detail, the novelties of the approach can be summarized as follows:

[11] 1. The problem is formally stated as extracting the maximum amount of information from D_I, by taking into account its final purpose (i.e., posing the question how to extract the maximum amount of information from D_I needed to do what is actually required); as a consequence, the truncation problem is fully accounted for.

[12] 2. An operator formalism is explicitly used to provide the links between the sources and the fields, effectively accounting for the a priori information on the (possibly disconnected) shape, size and radiating features of J, for the actual shape and size of D_I and D_O and for the characteristics of the measurement probe.

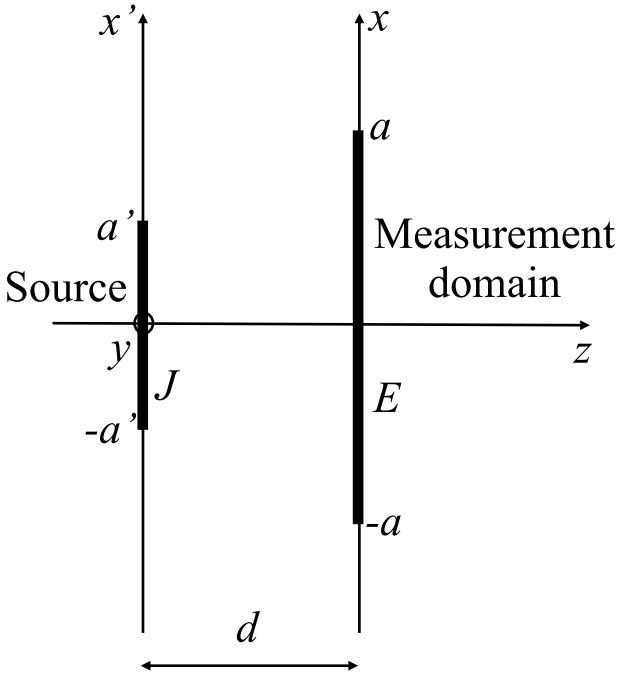

Figure 2. The case of parallel source and measurement domains.

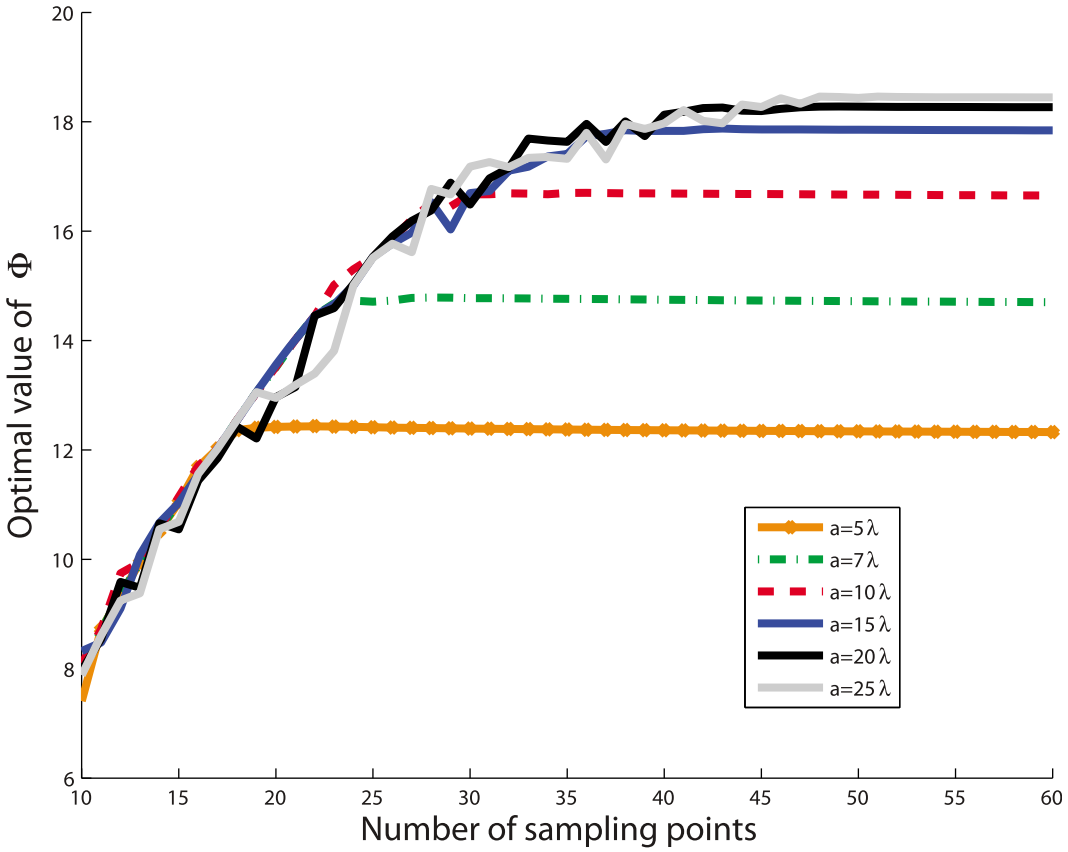

Figure 3. Choice of M for $a' = 7\lambda$ and $N = 32$.

[13] 3. Given the formalism based on linear operators, the answer is provided by exploiting, as a mathematical tool, the optimization of their singular value dynamics, in order to determine the field sample positions in D_I, then $\underline{J}_E$, and finally that part of the field on D_O predictable from measurements on D_I.

[14] 4. The generality of the approach allows handling also the very near field region of the source (i.e., sampling at fractions of the wavelength apart from the source, as is now more and more of interest in antenna characterization [*Ameya et al.*, 2009; *Capozzoli et al.*, 2009b] and inverse scattering [*Courjon*, 2003; *Bertero and De Mol*, 1996]) and nonanalytical domains D_I and D_O.

[15] The paper is organized as follows. In sections 2 and 3, the problem is formally introduced and formulated for a vector 3-D problem. In sections 4 and 5, the source subspace that can be reliably reconstructed from field samples, by properly defining samples number and locations, and the source subspace significantly contributing to the field, are analyzed. Section 6 presents an extensive numerical analysis in a 2-D setting of the approach for cases of practical interest in antenna radiation, by also comparing its performance with respect to that of the technique in [*Bucci and D'Elia*, 1996; *Bucci et al.*, 1998], since the latter has distinguished itself for exhibiting, till now, the most successful results. In particular, it is shown how the proposed technique has better sampling/interpolation/extrapolation capabilities. Furthermore, at variance with [*Bucci and D'Elia*, 1996; *Bucci et al.*, 1998], the proposed technique applies also to the case of very near field measurements and of measurements on nonanalytical domains. In section 7, the application of the method to a scalar 3-D case is outlined and shortly numerically illustrated. Finally, in section 8, conclusions are drawn and possible extensions are pointed out.

2. Problem

[16] Let us formally introduce the problem by referring to Figure 1, wherein: D_I is the domain from which the field information can be extracted; D_O is the (finite or

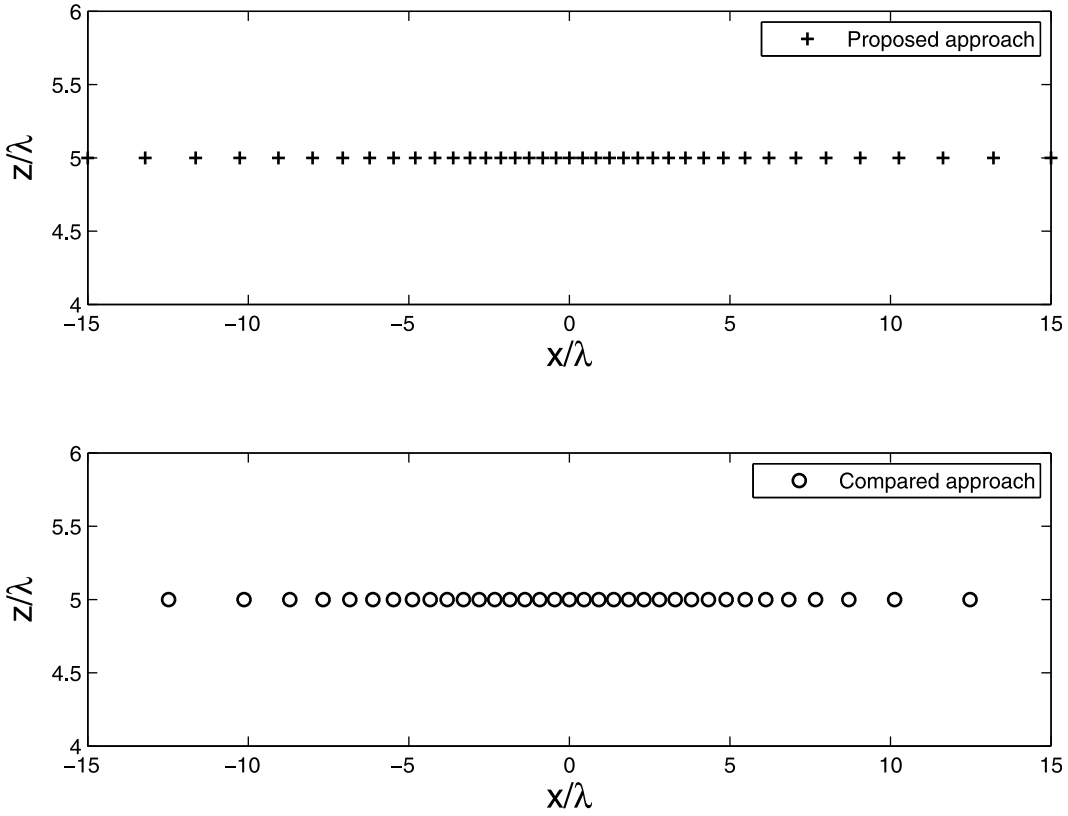

Figure 4. Sampling point locations when $N = 32$, $a = 15\lambda$, and $a' = 7\lambda$.

infinite, countable or uncountable) domain wherein the field should be estimated; $\underline{J}$ is the source; $\underline{J}_E$ is the subspace projection of $\underline{J}$ which can be estimated from D_I and has image on D_O; I_A is the available a priori information; I_I is the information gathered from D_I; I_O is the information, formed by I_I and I_A, and used to estimate the field on D_O; $\mathcal{A}_I$ and $\mathcal{A}_O$, are the radiation operators from the source $\underline{J}$ to D_I and D_O, respectively.

[17] The relationship between the field on D_I and that on D_O has been explicitly highlighted by the presence of $\underline{J}$ since, in practice, a priori information is available on its characteristics, as in the case when an estimate of its support and/or of its spectral content are available.

[18] Obviously, (1) I_I depends on the tool which can be employed to extract the information from D_I; (2) I_I should be submitted to its purpose through I_O. To clarify the above formal statements, let us discuss some simple examples of practical interest.

[19] Concerning point 1, i.e., the extraction of I_I from the field on D_I, a uniform or nonuniform sampling can be exploited, taking into account that the nonuniformity, defined on some a priori information on the geometry, can be properly worked out to improve the sampling efficiency and to control the effect of the noise [*Bucci and D'Elia*, 1996; *Bucci et al.*, 1998; *Vinetti*, 2008; *Capozzoli et al.*, 2009a]. Differently, the information throughput can be improved by using different probes, with different characteristics, as it happens in the case of phaseless measurements, wherein the information collected by the additional probe is accessed from the same domain to compensate for the lack of phase measurements [*Pierri et al.*, 1999].

[20] It is worth noting that the extraction process should account, in principle, for two needs, of which one could be privileged against the other depending on the particular requirements, i.e., on the expected results when reconstructing the field on D_O: improve effectiveness (amount of information) or improve efficiency (reduced redundancy).

[21] Concerning point 2, i.e., the reconstruction of the field on D_O, the reconstruction scheme should be tailored to the particular objective. For example, as long as D_O is a segment S, the reconstruction scheme should not be obtained from that used when D_O is a straight line containing S just after a trivial truncation.

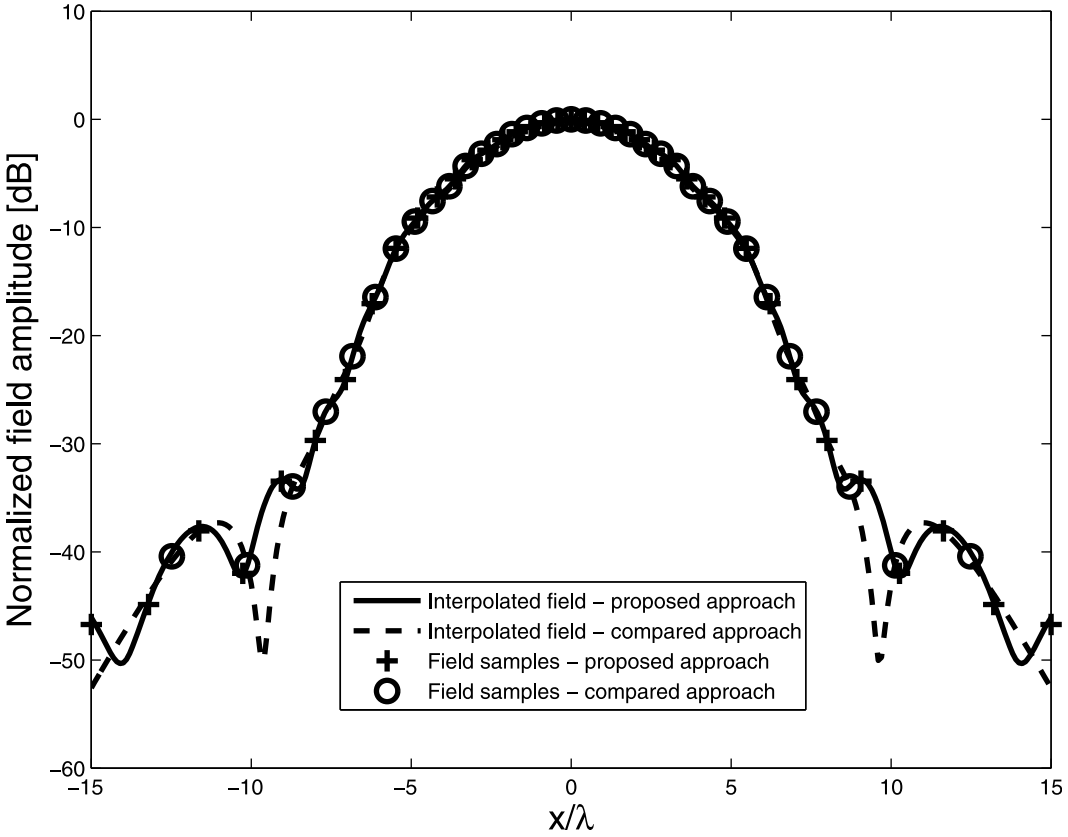

Figure 5. Field interpolation when $N = 32$, $a = 15\lambda$, and $a' = 7\lambda$. For the approach by *Bucci and D'Elia* [1996] and *Bucci et al.* [1998], $\chi' = \chi = 1.15$.

[22] It is worth noting that, the abstract framework introduced above includes some common issues as (1) field interpolation, when $D_O \subseteq D_I$ and D_O does not contain any field sample (belonging to D_I); (2) field extrapolation, when $D_O \cap D_I = \emptyset$ (disjoint domains), $D_O \supset D_I$ (prolongation), or $D_O \neq D_I$ and $D_O \cap D_I \neq \emptyset$.

3. Formulation of the Problem

[23] Figure 1 illustrates the vector radiation problem in which D_S is the domain containing the visible sources of the $\underline{E}$ field of interest (primary or scattered). Let us define $\underline{J}$ as the surface current, having support Γ, obtained from a single current formulation of the equivalence theorem applied to D_S filled with a perfect magnetic conductor [*Collin*, 1991].

[24] We consider an ideal probe acquiring the $\underline{E}$ field radiated on D_I at a number M of sampling positions. Herein, an ideal probe provides an output signal proportional to the field at the sampling point wherein the probe is located. Also nonideal probes could be considered, characterized by a more complex (linear) mapping between the field on D_I and the output signal to be processed [*Pierri et al.*, 1999]. The domains D_I and D_O are assumed arbitrary (in particular, possibly volumetric) and they will be specified depending on the particular cases of interest (see the tests discussed in section 6). We remark that, concerning the description of the source radiation, other representations, alternative to the considered one based on the equivalence theorem, can be exploited, such as multipole expansions or modal expansions (e.g., planar, cylindrical or spherical harmonics) without fictitiously increasing the number of degrees of freedom. The choice among these possibilities depends on the convenience for the particular problem of interest. In this paper, the attention is focused on the case when the information is extracted from complex vector field measurements on D_I [*Piestun and Miller*, 2000].

[25] Assuming the $exp(j\omega t)$ time dependence and that the medium surrounding D_S is homogeneous with dielectric permittivity ε and magnetic permeability μ, the relation between the source $\underline{J}$ and $\underline{E}(\underline{\rho})$ is provided by the

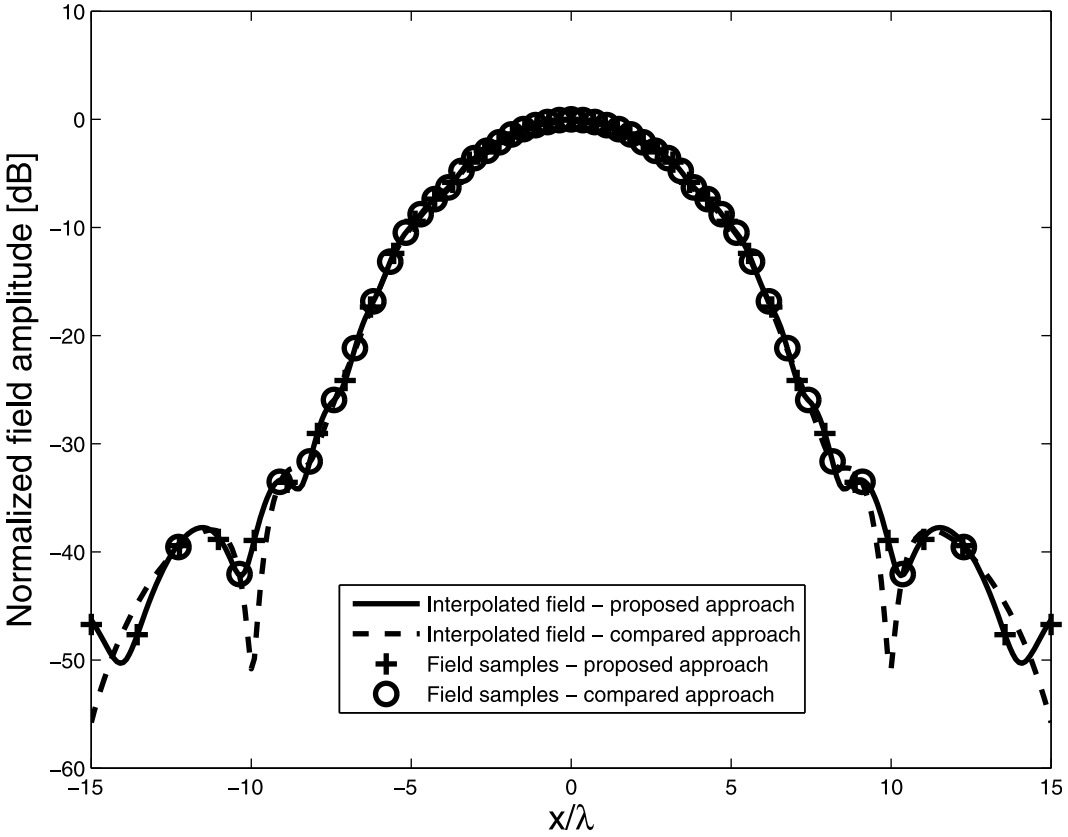

Figure 6. Field interpolation when $N = 32$, $a = 15\lambda$, and $a' = 7\lambda$. For the approach by *Bucci and D'Elia* [1996] and *Bucci et al.* [1998], $\chi' = \chi = 1.29$.

operators $\mathcal{A}_I$ and $\mathcal{A}_O$, depending on if the point of interest $\underline{\rho}$ belongs to D_I or D_O, respectively. In other words

$$\underline{E}\left(\underline{\rho}\right) = \begin{cases} \mathcal{A}_i(\underline{J}) & \underline{\rho} \in D_I \\ \mathcal{A}_O(\underline{J}) & \underline{\rho} \in D_O \end{cases}. \tag{1}$$

[26] The operators $\mathcal{A}_I$ and $\mathcal{A}_O$ are integral operators of the form

$$\underline{E}(\underline{\rho}) = -j\omega\mu\left[\underline{\underline{I}} + \frac{1}{\beta^2}\underline{\nabla\nabla}\cdot\right]\int_{\Gamma} \underline{J}(\underline{\rho}')G(\underline{\rho},\underline{\rho}')d\Gamma, \tag{2}$$

where $\underline{\rho}'$ denotes the source point, $G(\underline{\rho},\underline{\rho}')$ is the relevant Green's function accounting for the presence of the perfect conductor [*Collin*, 1991] and $\beta = \omega\sqrt{\varepsilon\mu}$ is the wave number, and will be specified in the following, depending on the case of interest. Obviously, the reported formulation as well as the approach that will be described next can be extended to magnetic currents on perfect electric conductors.

4. Source Reconstruction From Field Samples on a Domain

[27] In this section, we describe what about a source can be retrieved from field samples in a domain D, whose number M and spatial distribution are properly defined. As already stressed at the beginning of section 3, the use of an ideal probe is assumed, so that the information acquired on the field components of interest is pointwise. On the other side, the information collected by real sensors, on the condition that they are linear, is an "average" one involving the field values essentially around the considered sampling point. Therefore, the use of real probes has only a practical impact in affecting the kernel of the operator $\mathcal{A}_I$, the dealt with source reconstruction problem keeping linear. For NFFF transformation, accounting for the actual probe characteristics is known as "probe compensation" [*Paris et al.*, 1978].

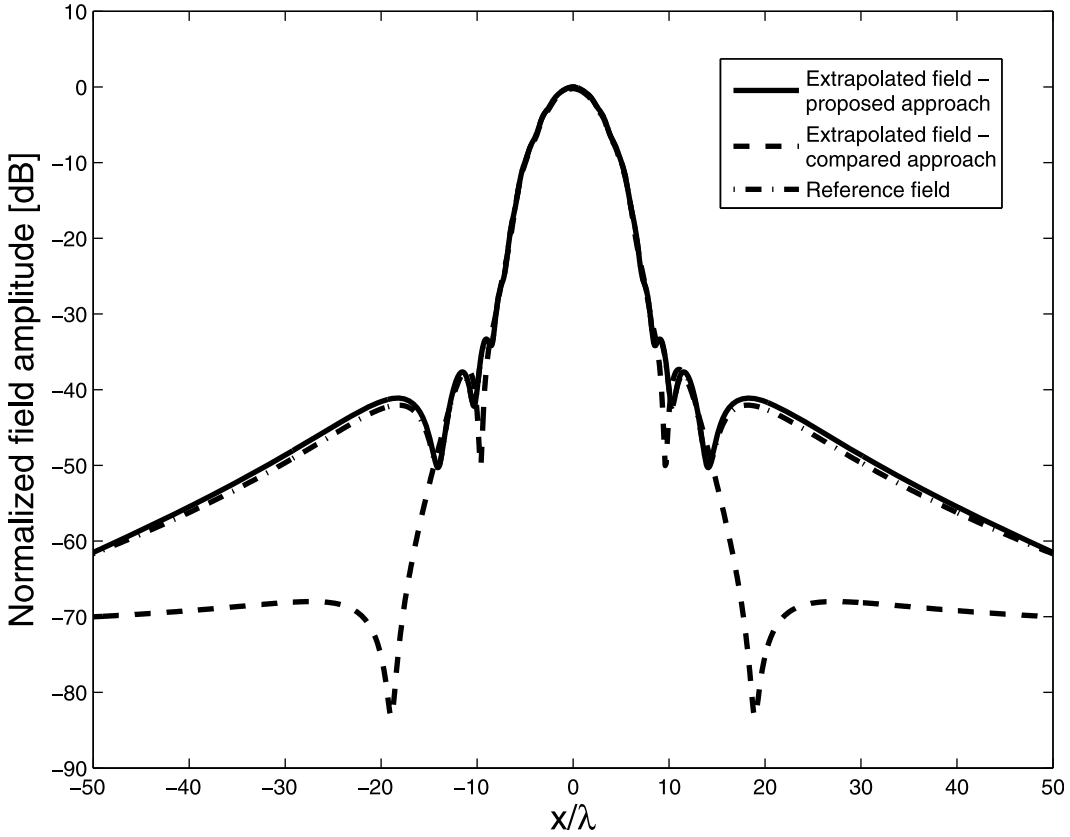

Figure 7. Field predicted on a measurement line set at $d = 5\lambda$ when $N = 32$, $a = 15\lambda$, and $a' = 7\lambda$.

Obviously, the results obtained here in a very general framework will be successfully used in the case of $\underline{J}$ and $\underline{J}_E$ and of the domains D_I and D_O.

4.1. Source Reconstruction by Singular Value Decomposition

[28] As a priori information on the source, we assume: (1) the spatial support of $\underline{J}$ and the adopted Green's function; (2) that $\underline{J}$ belongs to the (finite dimensional) subspace spanned by an orthonormal set of $N\,L^2$ functions $\{\underline{\psi}_n\}_{n=1}^{N}$, which will represent later on the subspace of "real interest" or just the "visible" subspace (see section 4.3). Obviously, more sophisticated Sobolev spaces [*Adams and Fournier*, 2003] could be considered to help enforcing some a priori known features (e.g., smoothness) during the reconstruction of the source. For examples of use of Sobolev spaces in image processing, see *Chan et al.* [2003].

[29] Thus, we set

$$\underline{J} = \sum_{n=1}^{N} I_n \underline{\psi}_n. \tag{3}$$

Accordingly, and taking into account that $\underline{E}$ is sampled at a number M of sampling points $\{\underline{\rho}_m\}_{m=1}^{M}$ on the domain D at hand, equation (1) can be recast as:

$$\underline{V} = \underline{\underline{Z}}\,\underline{I}. \tag{4}$$

[30] In equation (4), $\underline{V}$ is the column vector containing the vector components of the samples $\underline{E}_m$ of the field at $\underline{\rho}_m$ over some (say, P) unit vectors $\hat{i}_p$ ($\underline{\rho}_m$) defining the $\underline{E}$ field component of interest. In other words, the elements of $\underline{V}$ are the PM terms $\underline{E}_m \cdot \hat{i}_p$ and have a column ordering. Moreover, the elements of the $PM \times N$ matrix $\underline{\underline{Z}}$ are

$$\hat{i}_p \cdot \mathcal{A}_I\left(\underline{\psi}_n\right)\Big|_{\underline{\rho}=\underline{\rho}_m}. \tag{5}$$

[31] Finally, $\underline{I}$ is the vector of the I_n's. For fixed sample number M and locations, the problem of recovering $\underline{I}$ from $\underline{V}$ can be tackled by using a regularized (generally numerical) procedure based on the Singular Value Decomposition (SVD) approach [*Twomey*, 1965; *Jones*,

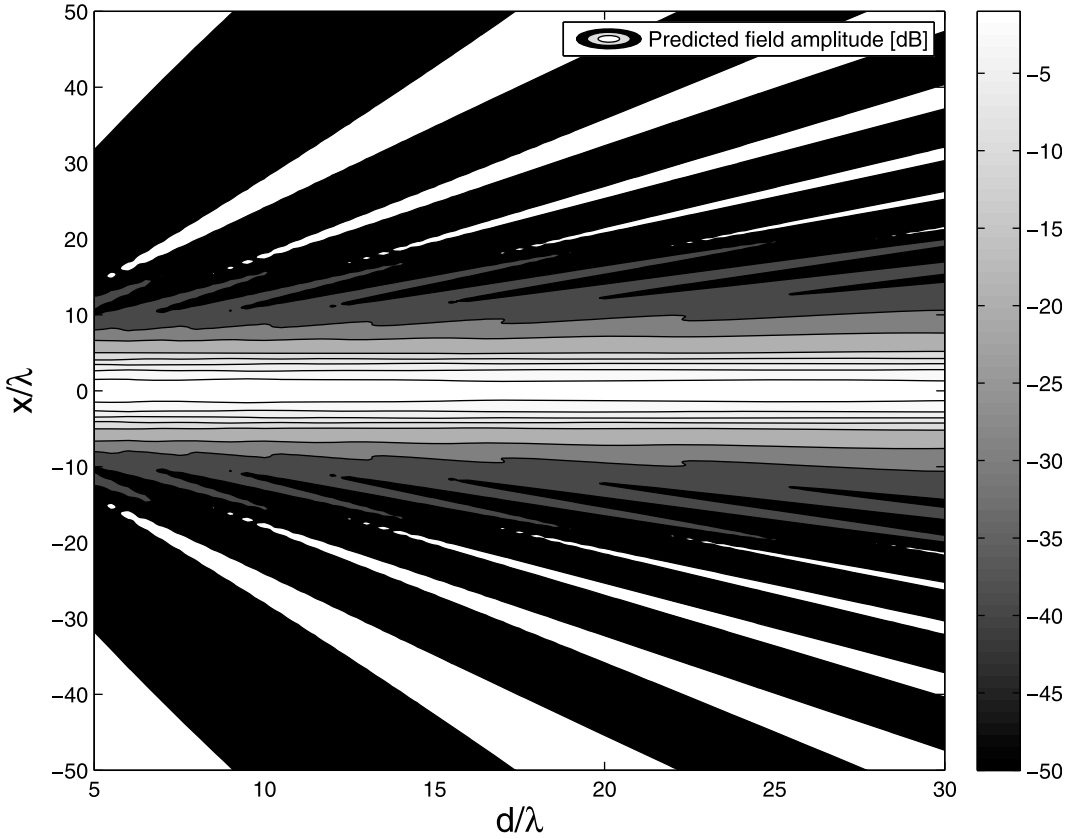

Figure 8. Field predicted on a region D_O with $-50\lambda \le x \le 50\lambda$ and $5\lambda \le z \le 30\lambda$ when $a' = 7\lambda$, $a = 15\lambda$, and $N = 32$.

1995; *Pierri and Soldovieri*, 1998]. In this paper, a Truncated SVD (TSVD) approach is employed [*Twomey*, 1965; *Jones*, 1995; *Pierri and Soldovieri*, 1998]. On assuming PM and N of the same order of magnitude, the computational cost of such procedure is N^3 [*Golub and Van Loan*, 1996].

4.2. Optimal Samples Number and Locations

[32] According to the theory of the TSVD approach, just the components of the source belonging to a vector subspace can be reliably retrieved. Furthermore, the matrix $\underline{\underline{Z}}$ is not univocally defined, since it depends on the choice of the vector subspace $\{\underline{\psi}_n\}_{n=1}^N$ and of both M, the number of sampling points, and the samples distribution. In other words, we have at our disposal a family of matrices $\underline{\underline{Z}}$ with different behaviors of the singular values. Therefore, the inversion should be performed by exploiting the element of the family with "the most convenient" singular value behavior, i.e., that corresponding, for a given choice of the subspace $\{\underline{\psi}_n\}_{n=1}^N$ (see section 4.3), to the "best conditioning." To cope with this point, the solution of the linear inverse problem (4) should then be preceded by an optimization step leading to the best choice of both M and the sample locations.

[33] Let us discuss this point in more details, and consider the SVD of $\underline{\underline{Z}}$ whose singular values are denoted by σ_k, with $k = 1, \ldots, K$ and $K = \min\{M, N\}$ [*Chan et al.*, 2003]. The behavior of the σ_k affects the amount of information conveyed on $\underline{I}$ by $\underline{V}$ [*McWhirter and Pike*, 1978; *Pike et al.*, 1984]. From this point of view, among all the matrices $\underline{\underline{Z}}$ of the family defined in equations (4) and (5) and for a fixed M, it is convenient to choose the locations of the sampling points providing the "flattest" singular values behavior (optimization of the generalized Shannon number [*Gori and Guattari*, 1973; *Piestun and Miller*, 2000]). (Different measures could be considered [see, e.g., *Curtis*, 2002].) And so, for a fixed M, the functional Φ [*Curtis*, 2002]

$$\Phi(\sigma_1, \ldots, \sigma_K) = \sum_{k=1}^{K} \frac{\sigma_k}{\sigma_1} \tag{6}$$

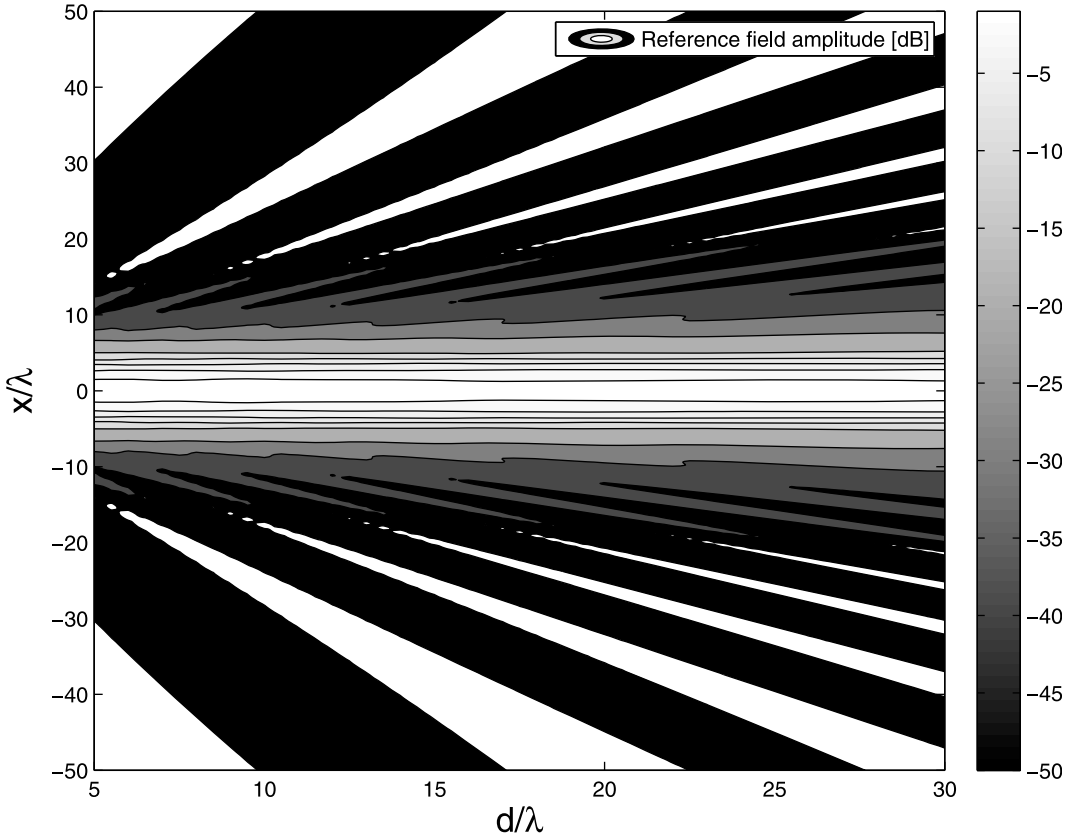

Figure 9. Exact field over the region D_O with $-50\lambda \le x \le 50\lambda$ and $5\lambda \le z \le 30\lambda$.

evaluating the "area" subtended by the normalized singular values σ_k/σ_1, is maximized. Obviously, for a fixed M, Φ is upper bounded by K.

[34] Let us now discuss the choice of the "optimal" number of samples M by recalling that, as above mentioned, Φ admits a meaningful interpretation in terms of generalized Shannon number [*Gori and Guattari*, 1973; *Piestun and Miller*, 2000]. This is recognized as a measure of the information on $\underline{I}$ gained from the knowledge of the field samples $\underline{V}$ in D. Then, on denoting by $\Phi_{opt}(M)$ the optimum of Φ for a given value of M, we expect that adding further sampling points constrained to belong to D (i.e., increasing M) will increase $\Phi_{opt}(M)$ until the maximum amount of information which can be gathered from D is reached. Beyond this condition, no further information can be conveyed on $\underline{I}$ by any newly added field sample (within D). Since $\underline{J}$ belongs to a finite dimensional space, this will correspond to the appearance of very small singular values and thus to a "saturation" behavior of $\Phi_{opt}(M)$ as a function of M [*Gori and Guattari*, 1973]. The number M at the saturation knee represents the minimum number of samples needed to achieve all the information available on I from the domain D.

[35] As a final remark, it is worth stressing that, once $\Phi_{opt}(M)$ saturates, the reconstruction of all the components I_n is not ensured. Accordingly, only a projection of $\underline{J}$ into the subspace S spanned by the acceptable singular vectors can be retrieved or, equivalently, only the elements of S have a significant image on the field on D. Obviously, S also depends on the criterion adopted for singular values truncation.

4.3. Source Representation

[36] In sections 4.1 and 4.2, we have described the role of the subspace S assuming that $\underline{J}$ belongs to a finite dimensional space spanned by (a priori known) basis functions $\underline{\psi}_n$'s. In particular, given D, S represents the subspace that can be reliably reconstructed from field samples on D, as well as the subspace significantly contributing to the field on D.

[37] Now, we have to define the $\underline{\psi}_n$'s according to the a priori information usually available. As already pointed

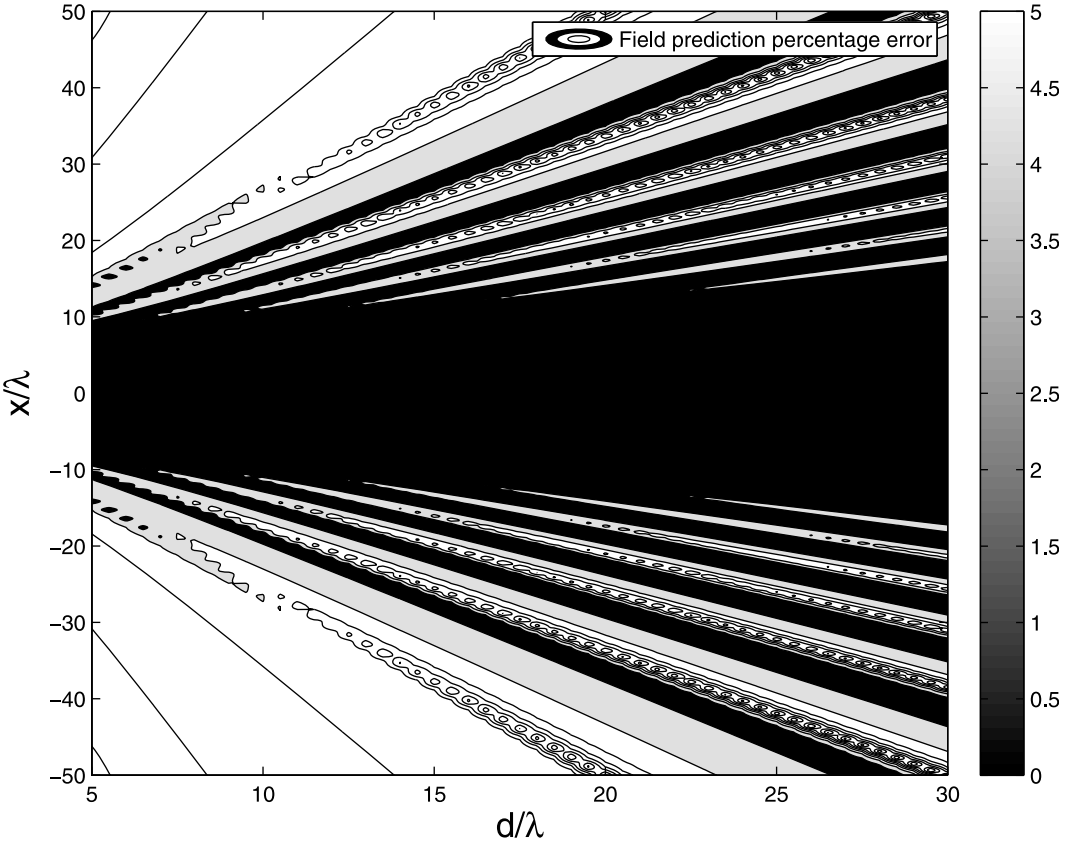

Figure 10. Percentage error of the field predicted over the region D_O with $-50\lambda \leq x \leq 50\lambda$ and $5\lambda \leq z \leq 30\lambda$.

out in section 4.1 and generally speaking, the $\underline{\psi}_n$'s can span the space (or a subspace thereof) of the "visible" (radiating) components of $\underline{J}$, which, as opposed to the "invisible" (nonradiating) space, does contribute to the radiated field [*Devaney and Wolf*, 1973; *Bleistein and Cohen*, 1977; *Devaney*, 2004]. The "visible" space can be analytically computed by the eigensolutions of the Helmholtz equation when D_S matches the geometry of an orthogonal reference system as, for example, a cylinder with circular cross section [*Chew et al.*, 1994] for a 2-D problem, a sphere [*Devaney and Wolf*, 1973; *Bleistein and Cohen*, 1977] or a (prolate or oblate) spheroid [*Sten*, 2004; *Sten and Marengo*, 2006, 2008] for a 3-D problem. Alternatively, the "visible" space can be analytically evaluated whenever particular symmetries of the source can be exploited [*Devaney and Marengo*, 1998]. In all the other cases, the $\underline{\psi}_n$'s can be determined as singular functions following a numerical procedure [*Salerno*, 1998].

[38] The attention of the remaining part of this paper (especially section 6) is focused on applications of the approach to antenna radiation and, in particular, to planar antennas. In NFFF transformations, for example, the interest is to reconstruct peculiar information about the source, as its radiated far field. Furthermore, in many cases of practical interest, the domain D_I is planar too, so that orthogonal field components of $\underline{E}$ bring information on orthogonal, and homologous, components of $\underline{J}$, and the problem becomes scalar. Accordingly, for the sake of simplicity, scalar radiation problems are henceforth considered. Furthermore, the attention is mainly devoted to the 2-D case (so that, $\underline{\rho} = (x, z)$), leaving the extension to a 3-D geometry in section 7. We underline that any extensions to scalar or possibly vector 3-D cases provides no conceptual difficulty, since the involved operators share the common property of compactness, so that the singular values decay to zero [*Piestun and Miller*, 2000]. Obviously, such extensions introduce additional computational load. A discussion thereof is provided in section 7.

[39] In the mentioned applications, the $\underline{\psi}_n$'s should be chosen so as to spanning a subspace of "real interest" for far-field reconstruction purposes. Also in many of these cases, the space of "real interest" can be analytically characterized as the eigenfunctions, or singular functions,

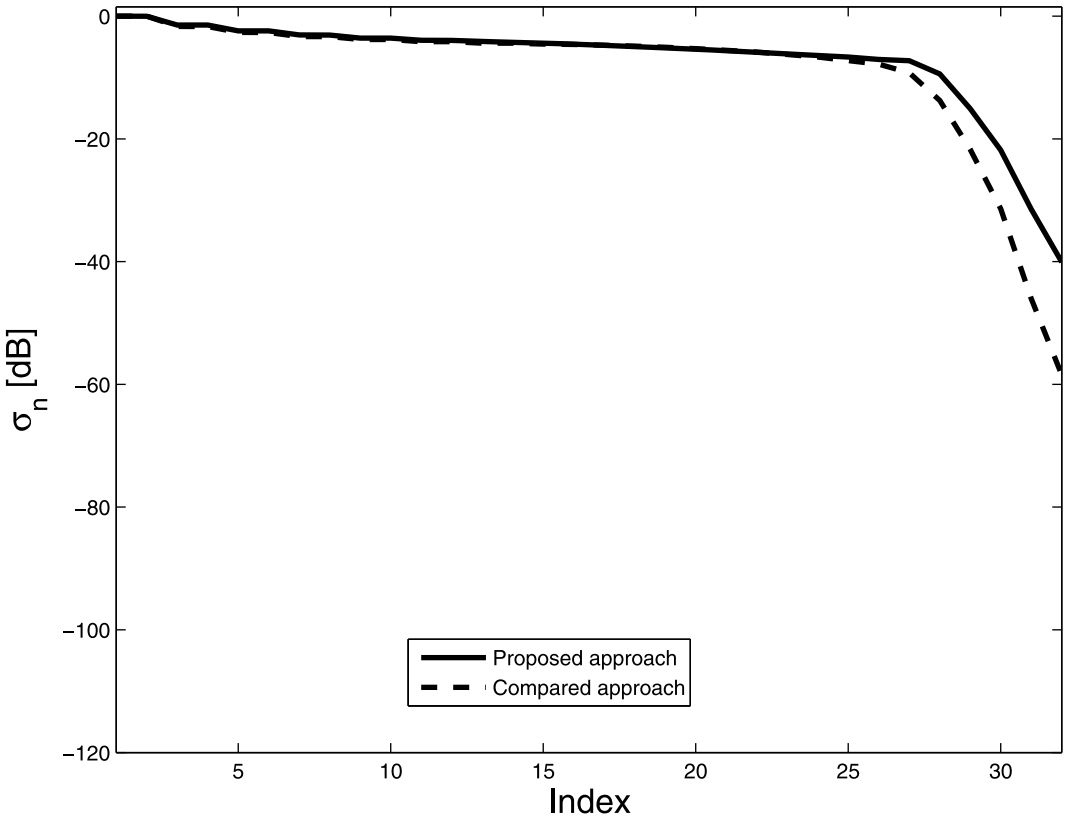

Figure 11. Singular values behavior when $N = 32$, $a = 15\lambda$, and $a' = 7\lambda$.

of a suitable operator. To this end, let us consider a case of significant interest in practical applications, i.e., that of a radiating strip, helpful for dealing with aperture antennas. In this framework, following the joint use of the equivalence theorem and image theory [*Collin*, 1991] (see Appendix A), $\underline{J}$ turns out to be tangent to the strip and to radiate in free space (see Figure 2). Accordingly, in a scalar setting when $\underline{J} = J\hat{i}_y$, the space of "real interest" is that spanned by the Prolate Spheroidal Wave Functions (PSWFs) [*Landau and Pollak*, 1962], i.e.:

$$J(x') = \sum_{n=0}^{N-1} I_n \Phi_n[c, x'] \tag{7}$$

where $\Phi_n[c, x']$ is the nth (normalized) PSWFs with space bandwidth product $c = \beta a'$ [*Landau and Pollak*, 1962] and a' is defined as in Figure 2. Indeed, J has a bounded support and is assumed to be nonsuperdirective [*Toraldo di Francia*, 1952; *De Villiers et al.*, 2001] so that only its radiative components (visible portion of the spectrum) are of interest to evaluate the field on domains at least "few" wavelengths apart from the source. Accordingly, it can be assumed that the current J has an essentially bounded spatial bandwidth and is well expanded as long as PSWFs with index $n < 4a'/\lambda$ are considered [*Landau and Pollak*, 1962]. Obviously, as long as domains in the VNF are considered, and as long as information on the amount of invisible spectrum is available, the expansion (7) should be extended also to some, known, PSWFs with index $n > 4a'/\lambda$.

5. Field Reconstruction

[40] Let us now turn our attention to the objective of the paper, we summarize here for the reader's convenience. The addressed problem consists in determining "at the best" the field on D_O from the knowledge of the field samples on D_I, given a priori information about the source.

[41] The above procedure consists of the following steps:

[42] 1. Given D_O and the $\underline{\psi}_n$'s selected along the guidelines of section 4.3, determine the subspace S_O (whose dimensions is N_O) of $\{\underline{\psi}_n\}_{n=1}^{N}$ having a significant image on the field on D_O; this step can be per-

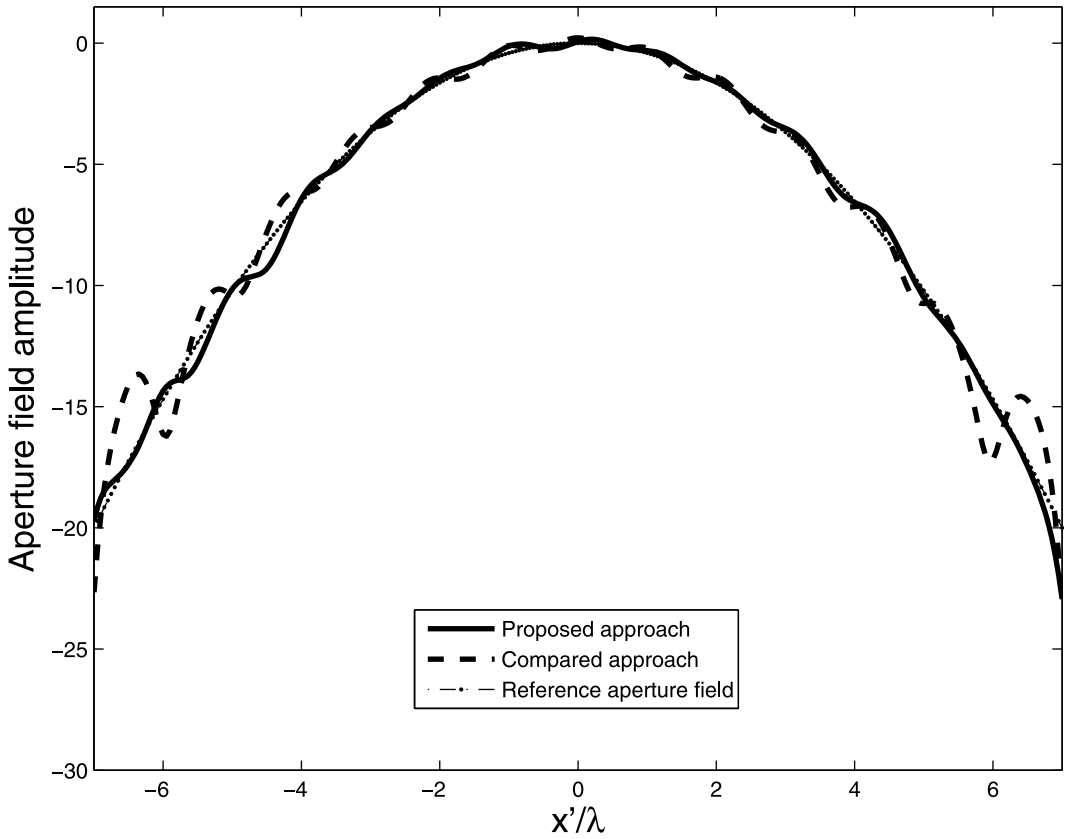

Figure 12. Reconstruction of the exponentially tapered source.

formed by means of the proposed SVD approach [*Jones*, 1995].

[43] 2. Given D_I and the $\underline{\psi}_n$'s again selected along the guidelines of section 4.3, determine the subspace S_I (whose dimensions is N_I) of $\{\underline{\psi}_n\}_{n=1}^{N}$ having a significant image on the field on D_I; also this step can be performed by the SVD approach.

[44] 3. Define $S_E = S_I \cap S_O$ and $\underline{J}_E$ as the projection of $\underline{J}$ on $S_E = S_I \cap S_O$.

[45] 4. Set $N_E = \dim(S_E)$.

[46] 5. If a local procedure is employed to optimize Φ, then set a starting guess for the number M and location $\{\underline{\rho}_m\}_{m=1}^{M}$ of the sampling points; such a starting guess can be provided by the approach of *Bucci and D'Elia* [1996] and *Bucci et al.* [1998], whenever applicable (see section 6.1).

[47] 6. Following the starting guess for M and $\{\underline{\rho}_m\}_{m=1}^{M}$, define a starting matrix $\underline{\underline{Z}}$ representing $\mathcal{A}_I$ from S_E to the sampling points.

[48] 7. Find M and $\{\underline{\rho}_m\}_{m=1}^{M}$ by optimizing the singular values behavior of $\underline{\underline{Z}}$.

[49] 8. Compute $\underline{J}_E$ from the field samples by a numerical regularized procedure based on the SVD approach [*Pierri and Soldovieri*, 1998].

[50] 9. Compute the field on D_O as $\mathcal{A}_O(\underline{J}_E)$.

[51] Obviously, from a practical point of view, the source reconstruction step from the field on D_I can be performed directly by finding the subspace of S_O having image on D_I, as it will occur for the presented numerical test cases.

6. Numerical Analysis

[52] In this section, we discuss several test cases illustrating the above procedure for the "optimal" choice of both M and the samples locations $\{\underline{\rho}_m\}_{m=1}^{M}$ and we show the performance of the proposed approach to reconstruct the field on D_O.

[53] First, a discussion concerning the way the functional Φ has been optimized, is presented. Then, the case of parallel source and near-field domains D_I and D_O (see Figure 2), a configuration of significant interest in NFFF transformations [*Yaghjian*, 1986; *Ameya et al.*, 2009;

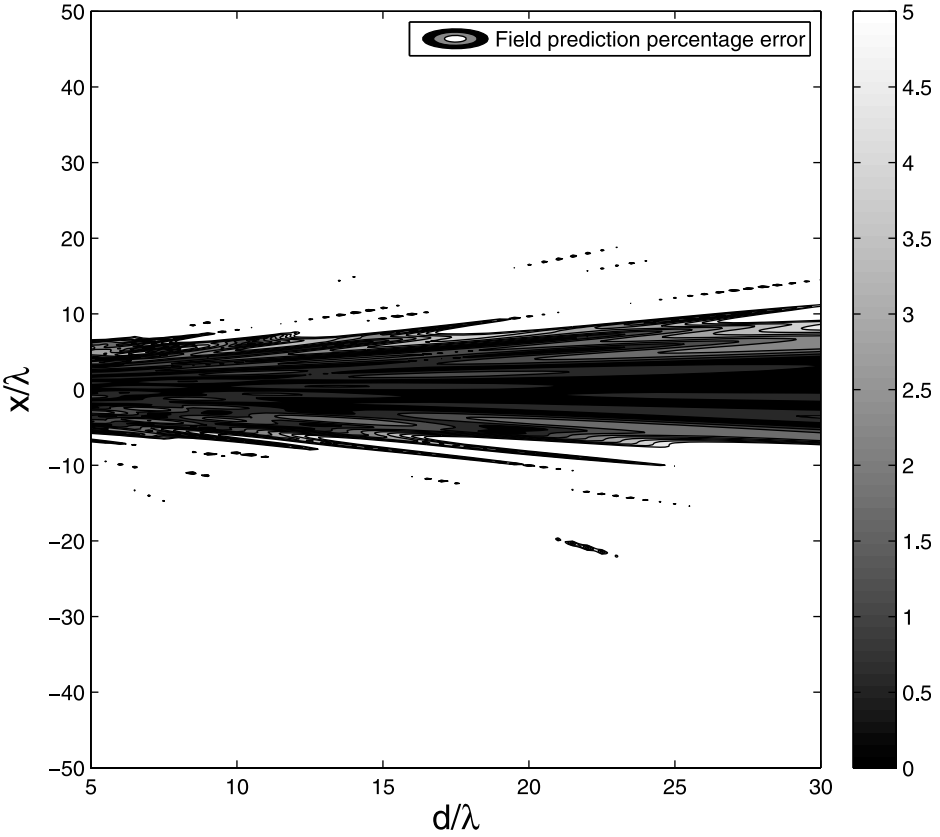

Figure 13. Percentage error of the field predicted over the region D_O with $-50\lambda \le x \le 50\lambda$ and $5\lambda \le z \le 30\lambda$, with noisy measurements and SNR = 40 dB.

Capozzoli et al., 2009b], is addressed, so that $\underline{\rho}_m = (x_m, z_m)$. The choice of the samples number and locations is discussed, for different sizes of the domains and for different amounts of a priori information, also by considering "electrically small" radiators. Field interpolation, field extrapolation and source reconstruction are illustrated also in presence of noise. Subsequently, the case of domains D_I.and D_O.in the very near-field region of the source is analyzed. Sources radiating tilted beams and nonanalytical domains are also dealt with. Much part of the analysis is carried out for the scalar, 2-D problem of a strip source with y-directed current distribution already mentioned in section 4.3. The case of arbitrarily polarized source is nevertheless briefly pointed out.

[54] As already mentioned in section 1, the performance of the approach is compared to that achievable by an alternative one, employing the technique of *Bucci and D'Elia* [1996] and *Bucci et al.* [1998] to select the sampling points, and retaining the use of the (regularized) SVD method. Finally, the case of a circular domain D_S is also numerically illustrated.

6.1. Optimization of Φ

[55] To fully specify the method, the procedure for the maximization of Φ must be defined. Obviously, since the maximization of Φ is a nonconcave problem [*Tuy*, 1998], a global optimization approach [*Capozzoli and D'Elia*, 2006] should be considered. However, even without the use of a global optimization algorithm capable to determine the global maximum of Φ, the use of a local optimization procedure employing, as a starting guess, the approach by *Bucci and D'Elia* [1996] and *Bucci et al.* [1998] would represent improvements thereof. In other words, a local optimization having, as starting point, the sampling by *Bucci and D'Elia* [1996] and *Bucci et al.* [1998] (when available) would necessarily lead to a better conditioned problem. Accordingly, the maximization of Φ has been performed by a gradient-based optimization procedure, adopting a multistep optimization approach gradually increasing the number of unknowns [*Pierri et al.*, 1999], and starting from the sampling points provided by *Bucci and D'Elia* [1996] and *Bucci et al.* [1998], whenever the theory by *Bucci and D'Elia* [1996]

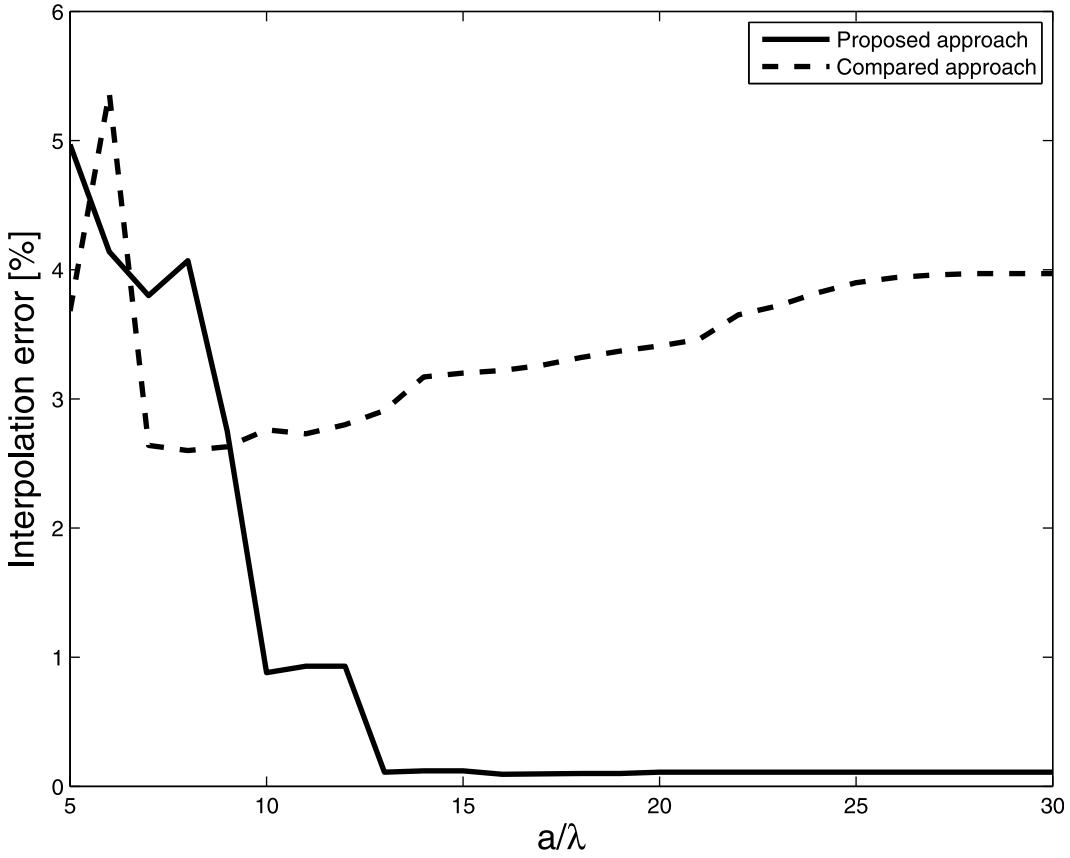

Figure 14. Interpolation errors (%) when $N = 32$, and $a' = 7\lambda$ for different values of a.

and *Bucci et al.* [1998] applies. In all the other cases, uniform sampling has been adopted as starting guess.

[56] In order to improve the effectiveness and the efficiency, reducing the overall number of involved parameters, the abscissas x_m are represented as [*Capozzoli et al.*, 2008, 2009c]

$$x_m = \sum_{k=0}^{K-1} c_k P_k(\xi_m), \;\; m = 1, ..., M \;, \tag{8}$$

where the ξ_m are uniformly spaced within $[-1,1]$, P_k are basis functions, and c_k are the expansion coefficients. The representation (8) maps a set of M, uniformly spaced abscissas ξ_m into a set of M, nonuniformly spaced abscissas x_m in such a way that only the few c_k's can be considered as parameters to be optimized. Accordingly, the basis functions P_k should be suitably chosen to allow a significant reduction of the number of unknowns to be determined while optimizing Φ. Since we expect that the local sampling step of the field smoothly changes from point to point, a polynomial (e.g., Legendre or Chebyshev) expansion involving few (3 or 4) terms is generally sufficient to provide an adequate representation of the sampling points, as it has been observed also with reference to other, different (e.g., the design of Plane Wave Synthesizers) applications [*Capozzoli et al.*, 2009c]. For the examples of section 6, Legendre polynomials with $K = 3$ have been exploited, by also verifying that a further enlargement of the number of unknowns does not give rise to appreciable improvements in the field sample positions.

[57] We remark that, the optimization of functional Φ requires, at each iteration step, the numerical evaluation of the singular values of $\underline{\underline{Z}}$. With regard to this, it should be noticed that, on assuming once again PM of the same order of magnitude of N, the computational burden for a full evaluation of the SVD of $\underline{\underline{Z}}$ grows as $O(N^3)$ [*Golub and Van Loan*, 1996]. However, Φ requests the only singular values whose computation is, in general, less demanding than the calculation of a full SVD. The optimization procedure of Φ developed in the present paper adopts a particularly efficient and accurate LAPACK

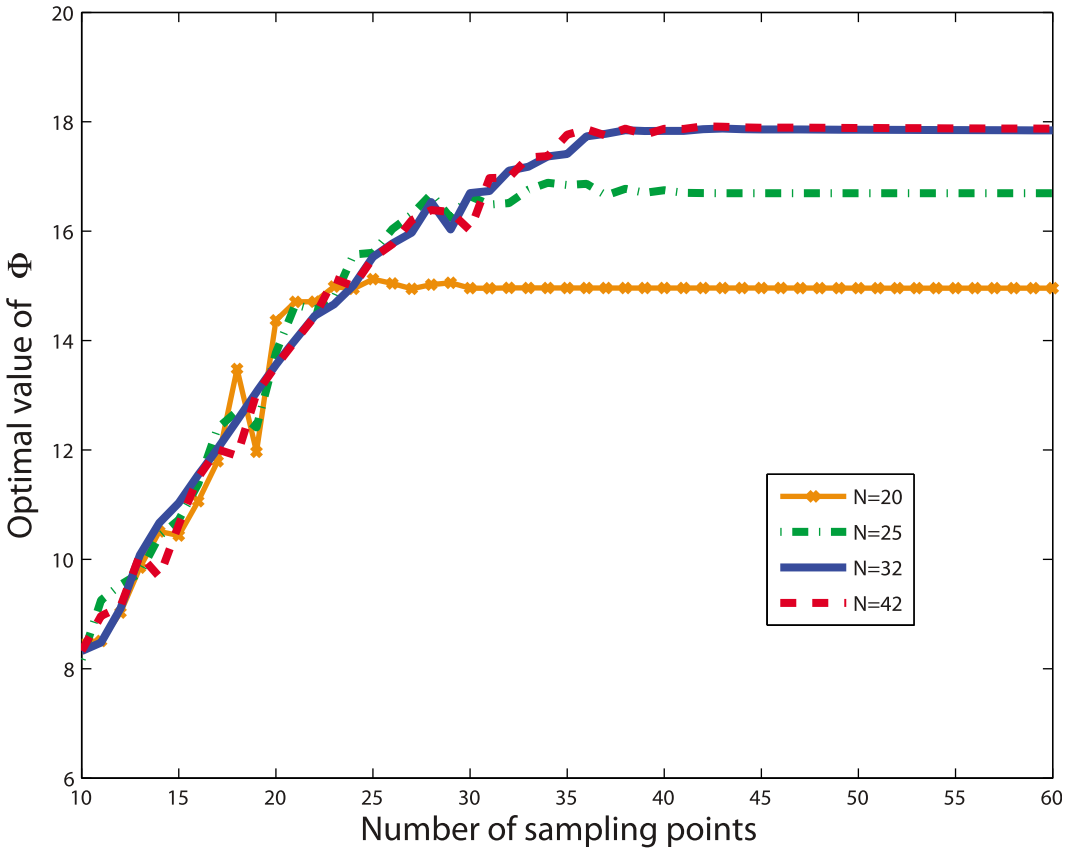

Figure 15. Choice of M for $a' = 7\lambda$ and $a = 15\lambda$.

scheme [Netlib], detailed by *Fernando and Parlett* [1994], for the evaluation of only the singular values.

[58] It is finally worth noting that, despite the linearity of the inverse problem, the determination of the sampling points leads to the preventive solution of a nonlinear one, as required it happens in any preliminary, and unavoidable, discretization process.

6.2. Parallel Source and Near-Field Measurement Domains

[59] Let us now consider the case of parallel measurement and source domains with $\underline{J} = J\hat{i}_y$ (see Figure 2). In this case, $D_I = D_O$ and the operators $\mathcal{A}_I$ and $\mathcal{A}_O$ can be expressed as

$$E(x)\hat{i}_y = \mathcal{A}_I\left(J\hat{i}_y\right) = \mathcal{A}_O\left(J\hat{i}_y\right) = -\frac{\omega\mu}{4}\int_{-a'}^{a'} J\left(x'\right)\hat{i}_y H_0^{(2)}(\beta R)dx', \quad (9)$$

where $E(x)\hat{i}_y$ is the only nonvanishing component of the field [*Tai*, 1993], $R = \sqrt{(x-x')^2 + d^2}$ and $H_0^{(2)}$ is the Hankel function of zeroth order and second kind. The distance d between the two domains is set equal to 5λ.

6.2.1. Choice of M, Given N, a, and a'

[60] The blue line in Figure 3 illustrates, for $N = 32$, $a = 15\lambda$ and $a' = 7\lambda$, the choice of the number M of sampling points by depicting the optimal values of Φ, say $\Phi_{opt}(M)$, as a function of M. The value of N corresponds to the number of all the "visible" PSWFs, i.e., $N \approx 4a'/\lambda$. As it can be seen, according to the considerations made in the previous sections, as the number of sampling points located in the interval $[-a, a]$ increases, the functional Φ increases until it reaches a saturation level.

[61] Then, the number M of sampling points can be chosen as the one corresponding to the saturation knee, i.e., $M = 43$ in the actual example. We remark that the considered number N, here a priori fixed, depends, in the general case, on both, the a priori information on the source as well as on the considered domain D_O. For the

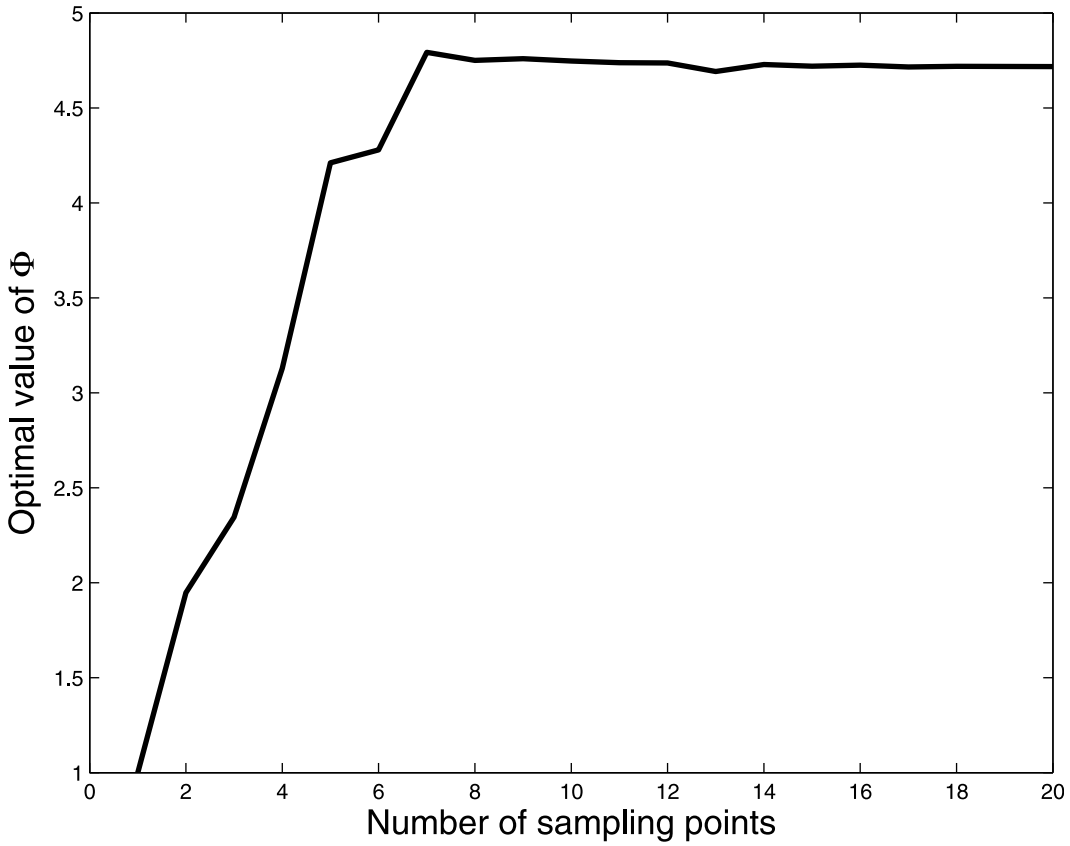

Figure 16. Choice of M for $a' = 1\lambda$, $a = 10\lambda$, and $N = 12$.

considered test case, $N = N_I$ since the whole "visible" components of J are involved and retrievable from D_I.

6.2.2. Choice of the Sampling Point Distribution, Given N, a, and a'

[62] Figure 4 shows, for the same case considered above, the obtained locations of the sampling points along with the sampling points as obtained by *Bucci and D'Elia* [1996] and *Bucci et al.* [1998]. As it can be seen, the latter involves less points (in particular, 35), but the intersampling spacing at the edges of the measurement domain becomes large, which will lead to a significant interpolation error due to truncation.

[63] It should be remarked that the first $K = 3$ expansion coefficients of the Legendre polynomials determined, by the proposed method, for the representation of the sampling points have been $c_1 = 0.803$, $c_2 = 0.2109$ and $c_3 = 0.0042$. It has been also verified that the search for further Legendre polynomials would not significantly change the sampling point locations as compared to the result in Figure 4 due to lower and lower coefficients c_k.

[64] It should be noticed that the number of 35 field samples is determined, according to the procedure pointed out by *Bucci and D'Elia* [1996] and *Bucci et al.* [1998], (1) starting from the sampling points falling on an infinite line and then selecting those lying on the $(-a, a)$ segment; (2) defining band limitation and oversampling (as compared to the Nyquist step) control factors χ' and χ, respectively; for the considered cases, following the choice by *Bucci et al.* [1998], they have been fixed to $\chi' = \chi = 1.15$.

[65] Accordingly, the information on the size of the measurement domain is "weakly" accounted for by *Bucci and D'Elia* [1996] and *Bucci et al.* [1998], and the truncation error is generally controlled by acting on χ and χ' and on the use of proper windowing functions.

[66] On the other side, the proposed procedure involves more points (i.e., 43), but will allow a better handling of the sampling at the boundaries of $[-a, a]$. The better performance of the sampling at the edges of the measurement interval can be ascribed to both, the stronger information about the support of J and to the explicit account for the image domain of $\mathcal{A}_I$. Obviously, the improvement is obtained at the cost of a heavier computational burden.

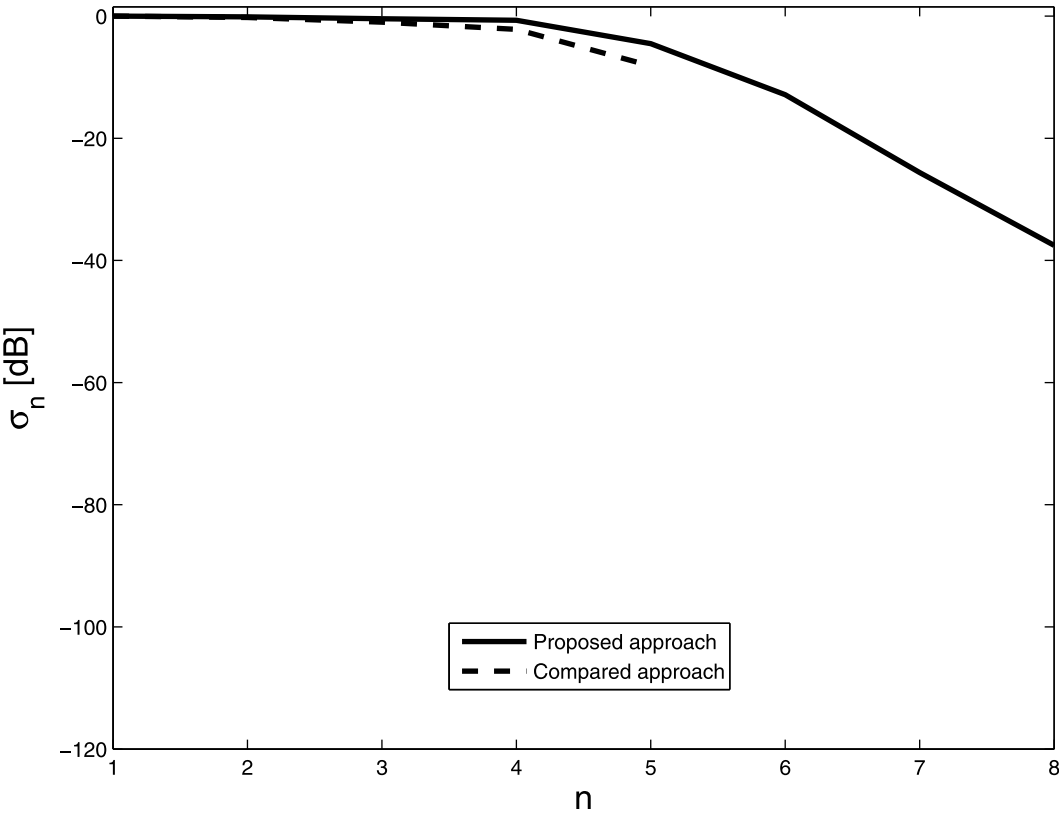

Figure 17. Singular value behavior for $a' = 1\lambda$, $a = 10\lambda$, and $N = 12$.

6.2.3. Field Interpolation

[67] In this case we considered a source uniform in phase and exponentially tapered with taper equal to 20 dB. Furthermore, we set $D_I = D_O$ so that $N = N_I = N_O = N_E$. Figure 5 shows the field interpolated (i.e., the field estimated on D_O when $D_I \equiv D_O$) according to the proposed interpolation procedure as well as the field interpolated according to *Bucci and D'Elia* [1996] and *Bucci et al.* [1998]. The root mean square interpolation error has been equal to 0.11% for the proposed approach and to 3.2% for the approach by *Bucci and D'Elia* [1996] and *Bucci et al.* [1998]. A "traveling" interpolation has been considered [*D'Elia et al.*, 1985] for this last approach.

[68] To provide a more balanced comparison, Figure 6 shows the field interpolated according to the proposed interpolation procedure as well as the field interpolated according to *Bucci and D'Elia* [1996] and *Bucci et al.* [1998] when the control factors are chosen equal to $\chi' = \chi = 1.29$ in order to have a number of 43 samples within $(-a, a)$, i.e., the same number of M samples determined by the procedure in section 4.2. By comparing Figures 5 and 6, the performance of *Bucci and D'Elia* [1996] and *Bucci et al.* [1998] keeps practically unchanged so that the approach here proposed appears to be more convenient.

6.2.4. Field Extrapolation

[69] In this case, we set $D_O \supset D_I$. Accordingly, since $N_I = N$, then $N = N_I = N_O = N_E$. Figure 7 depicts the near field for the same test case as above. Again the results of the proposed approach and the ones based on *Bucci and D'Elia* [1996] and *Bucci et al.* [1998] are reported. As it can be seen, exploiting the a priori information on the radiating source (equation (7)) guarantees a roll-off outside D_I closer to the actual near field than the one corresponding to the approach [*Bucci and D'Elia*, 1996; *Bucci et al.*, 1998].

[70] Since $N = N_E$, in confirmation of the capability of the proposed approach to foresee the field outside the measurement region D_I, a region D_O such that $-50\lambda \le x \le 50\lambda$ and $5\lambda \le z \le 30\lambda$ is considered. Figures 8–10 illustrate the field predicted on D_O, the exact field, and the percentage prediction error, respectively. As seen, the percentage error keeps very low in the region of high field intensity, while staying below 30% for the regions involving the field sidelobes.

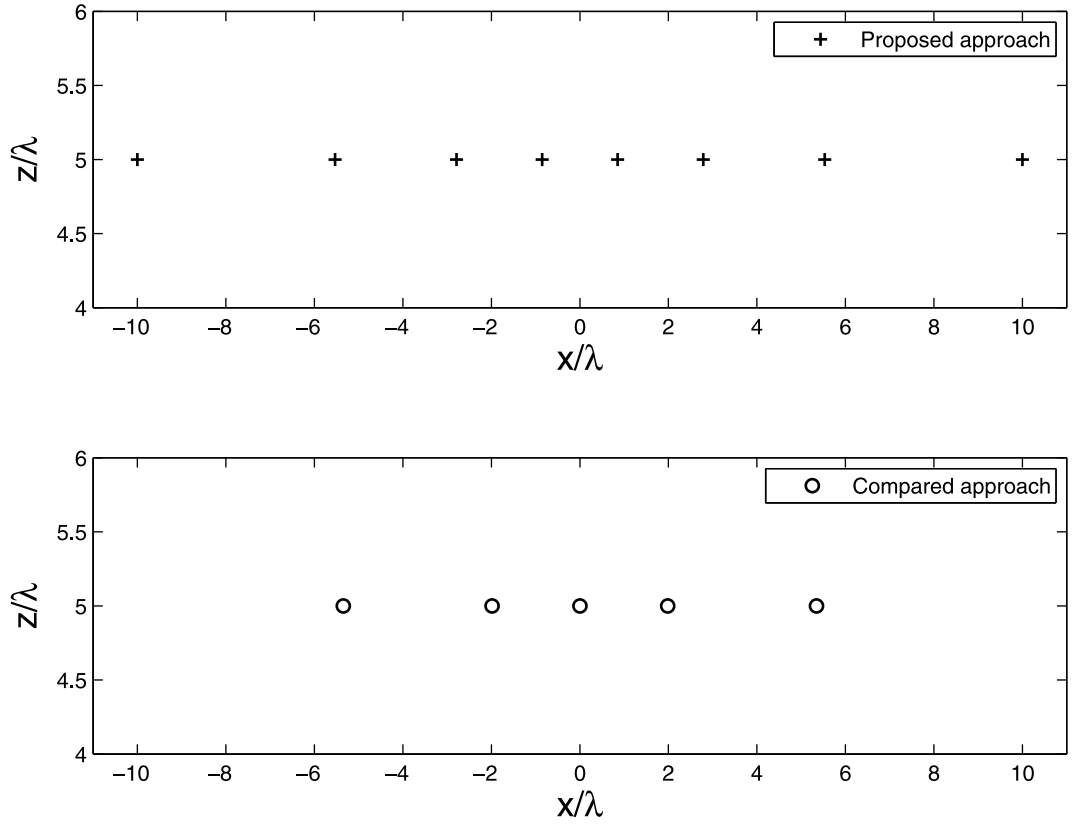

Figure 18. Sampling point locations for $a' = 1\lambda$, $a = 10\lambda$, and $N = 12$.

6.2.5. Source Reconstruction and Field Extrapolation in Presence of Noise

[71] Figures 11 and 12 depict the singular values behavior for the same case as for Figures 4–10 and the reconstruction of the exponentially tapered source, respectively. In particular, and concerning Figure 12, the dash-dot represents the actual source, the solid line the reconstruction by the present approach and the dashed line the reconstruction when the field is sampled according to the standard sampling theory. The obtained root mean square errors are 3.16% and 6.76% for the first and second case, respectively. A noise with a Signal-to-noise ratio (SNR) of 30dB has been superimposed to the field samples. Finally, Figure 13 depicts the same result as for Figure 10, when the data are corrupted by additive noise with a SNR = 40dB.

6.2.6. Choice of *M* as a Function of *a*, Given *N* and *a'*

[72] Figure 3 illustrates, for $N = 32$, $a' = 7\lambda$, and for various sizes of the measurement domain a, the choice of the number M of sampling points by depicting $\Phi_{opt}(M)$ for each value of a. As it can be seen, for all the cases, by increasing the number of sampling points in $[-a, a]$, the functional Φ increases until it reaches the saturation level, and again the number M of sampling points can be chosen as that corresponding to the saturation knee. Furthermore, by enlarging the size of the measurement domain, the number M of sampling points corresponding to the saturation knee of Φ tends, in turn, to saturate, as testified by the accumulation of the curves in Figure 3 for larger values of a.

[73] Finally, Figure 14 illustrates the achieved interpolation errors when $N = 32$, $a' = 7\lambda$ and for different values of a. As long as the measurement domain enlarges, the approach of *Bucci and D'Elia* [1996] and *Bucci et al.* [1998] exhibits worse performance as compared to the proposed one due to the "rarefaction" of the field samples at the edges of D_I.

6.2.7. Choice of *M* as a Function of *N*, Given *a* and *a'*

[74] Figure 15 now illustrates the choice of M when $a = 15\lambda$, $a' = 7\lambda$, and for different values of N. In this case, N no longer coincides with the number of "visible" PSWFs. As it can be seen, by increasing N, the value of M corresponding to the saturation knee increases until N equals 32, i.e., until N equals the number of all the visible

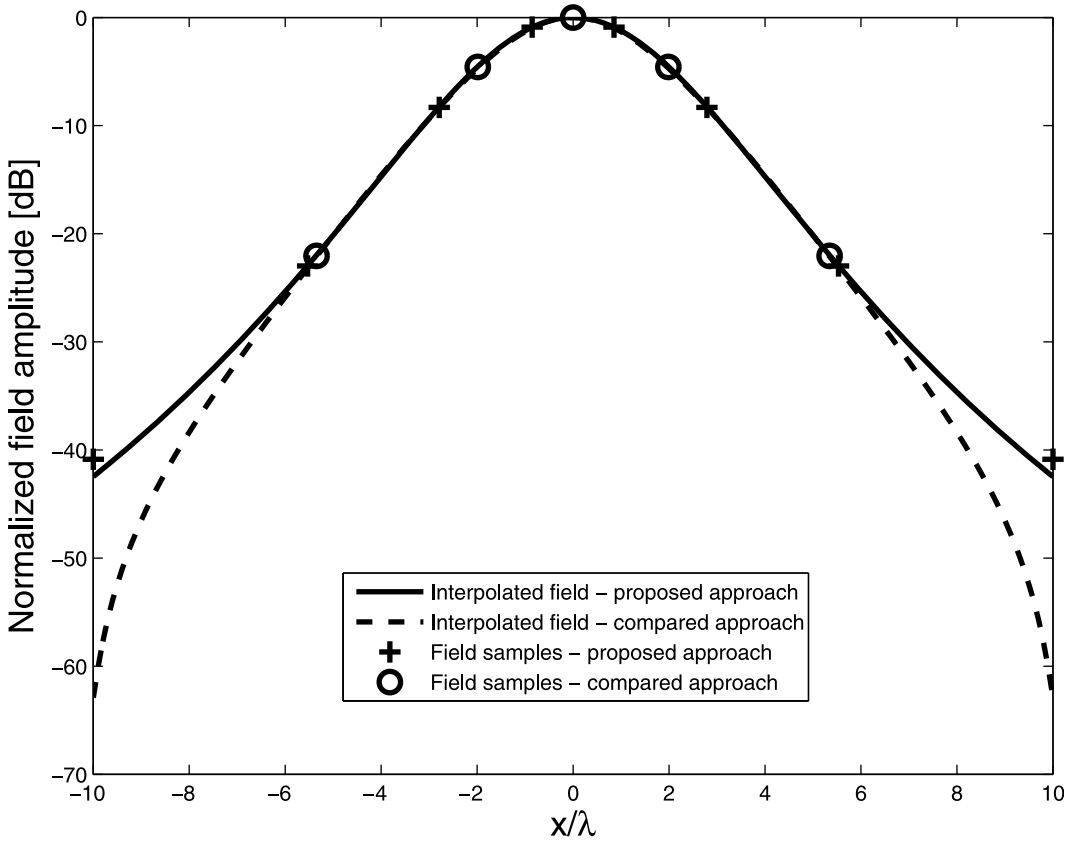

Figure 19. Field interpolation when $a' = 1\lambda$, $a = 10\lambda$, and $N = 12$.

PSWFs. Adding further PSWFs (contributing only to the near field) to the representation (7) of the source current, i.e., in the case $N = 42$ of Figure 15, the number M keeps practically unchanged and equal to the value corresponding to $N = 32$.

6.2.8. "Electrically Small" Sources

[75] Figures 16–18 illustrate the approach as applied to the case of an electrically small source with $a' = 1\lambda$, $a = 10\lambda$, and $N = 12 = 3{\cdot}4a'/\lambda$. In particular, Figure 16 depicts the choice of M, whereas Figures 17 and 18 further confirm the convenience of the approach, by comparing the singular values of $\underline{\underline{Z}}$ and the sampling locations for the presented approach and that by *Bucci and D'Elia* [1996] and *Bucci et al.* [1998], respectively. The improvement in the number of "useful" singular values can be clearly appreciated. Finally, for a source with the same exponential tapering considered above, Figure 19 compares the fields as interpolated according to the proposed interpolation procedure and the procedure by *Bucci and D'Elia* [1996] and *Bucci et al.* [1998].

6.2.9. Very Near Field Sampling

[76] We now consider the problem of determining the sampling points for the same geometry of Figure 2, when the measurement domain is in the very near field (VNF) region of the source [*Vinetti*, 2008]. In particular, a distance $d = 0.3\lambda$ is considered when $a = 15\lambda$ and $a' = 7\lambda$.

[77] Two cases are addressed. In the first one (case VNFa), $N = 32$, i.e., all the radiating PSWFs are involved in equation (7). In the second one (case VNFb), $N = 42$, i.e., a number of 10 more PSWFs giving rise to an evanescent VNF are further introduced in equation (7).

[78] Figures 20 and 21 show the choice of M and the singular values behavior for both the considered cases. As it can be seen from Figure 20, the optimal values of Φ exhibit a saturation behavior also for VNF measurements and such a saturation is reached when $M = 32$ for case VNFa and when $M = 42$ for case VNFb. Note how the number of sampling points for the former is smaller than that for the latter due to the smaller VNF bandwidth related to the missing evanescent part of the spectrum. Similarly, from Figure 21, it is seen that, as expected, the number of significant singular values of $\underline{\underline{Z}}$ is larger for case VNFb than VNFa. Finally, the larger VNF bandwidth of case VNFb as compared to that of case VNFa can be observed from the smaller mean sampling step, given by 0.35λ and 0.45λ, respectively (see Figure 22).

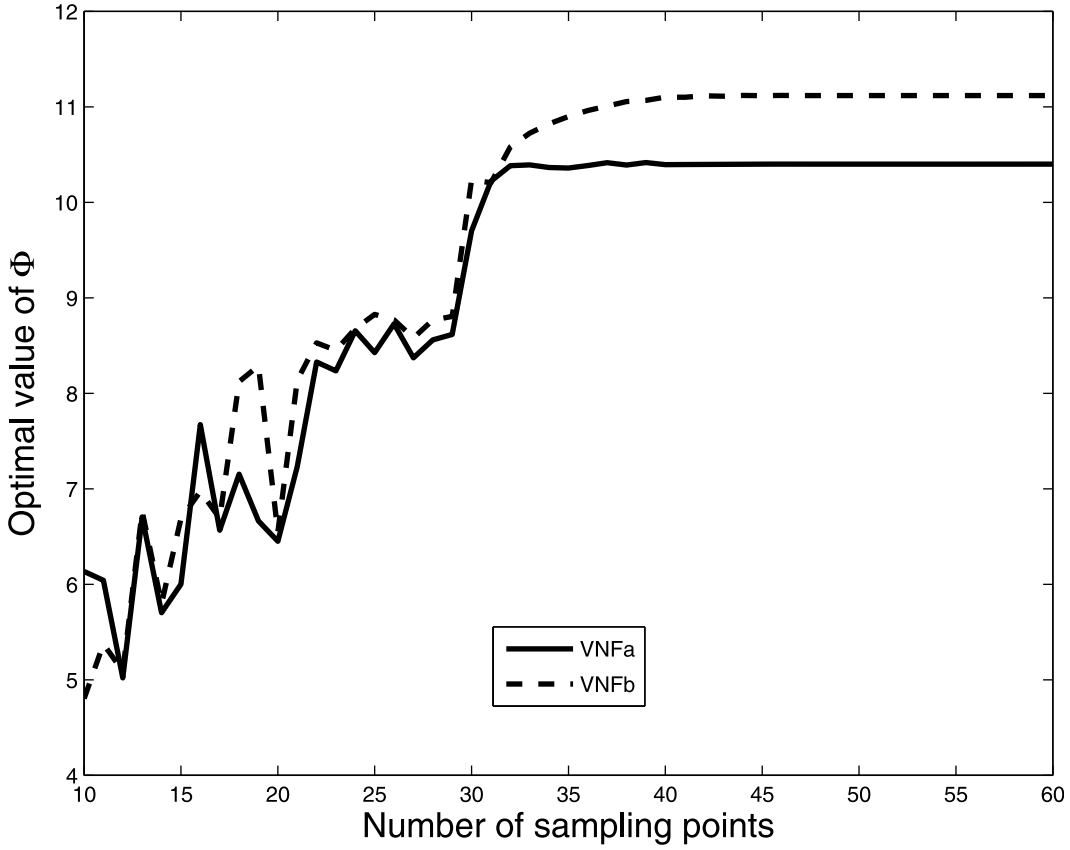

Figure 20. Illustration of the choice of M for VNF measurements.

We remark that, for all the test cases considered in this section, a uniform sampling has been considered as starting point for the optimization of Φ.

[79] Before moving to the next subparagraph, we would like to stress that the very near field sampling has relevant practical applications. Scanning Near-field Optical Microscopy (SNOM) [*Courjon*, 2003] and very near field antenna characterization systems [*Vinetti*, 2008] are just two of them.

6.2.10. An *x*-Directed Source

[80] Let us now briefly sketch the case of an x-directed current distribution $\underline{J} = J\hat{i}_x$. Also in this case, $D_I = D_O$ and the operators $\mathcal{A}_I$ and $\mathcal{A}_O$ can be expressed as

$$E(x)\hat{i}_x = \mathcal{A}_I\left(J\hat{i}_x\right) = \mathcal{A}_O\left(J\hat{i}_x\right) = -\frac{1}{4\omega\varepsilon}\int_{-a'}^{a'} J\left(x'\right)\hat{i}_x \frac{\partial^2 H_0^{(2)}(\beta R)}{\partial x^2}dx'. \quad (10)$$

[81] We here just point out that, the approach above illustrated with reference to equation (9) can be easily applied also to equation (10). On the other side, the case of a strip source can be equivalently managed by referring to the aperture field and its Plane Wave Expansion. This point of view should immediately convince the reader that polarization issues can be easily managed.

6.3. Source Radiating Tilted Beams and Nonanalytical Measurement Domains

[82] The last two test cases aim at proving the consistency and the flexibility of the approach. Let us deal first with the consistency. Up to now, we have shown its performance against currents radiating a "broadside" beam, so that we now address first the case of sources radiating a tilted beam due to a known linearly varying phase term on J. In other words, we assume that J is given by

$$J(x') = \left[\sum_{n=0}^{N-1} I_n \Phi_n[c, x']\right] \exp[-j(\beta \sin\alpha)x'], \quad (11)$$

where the angle α is known and determines the pointing direction of the far field pattern. Furthermore, the

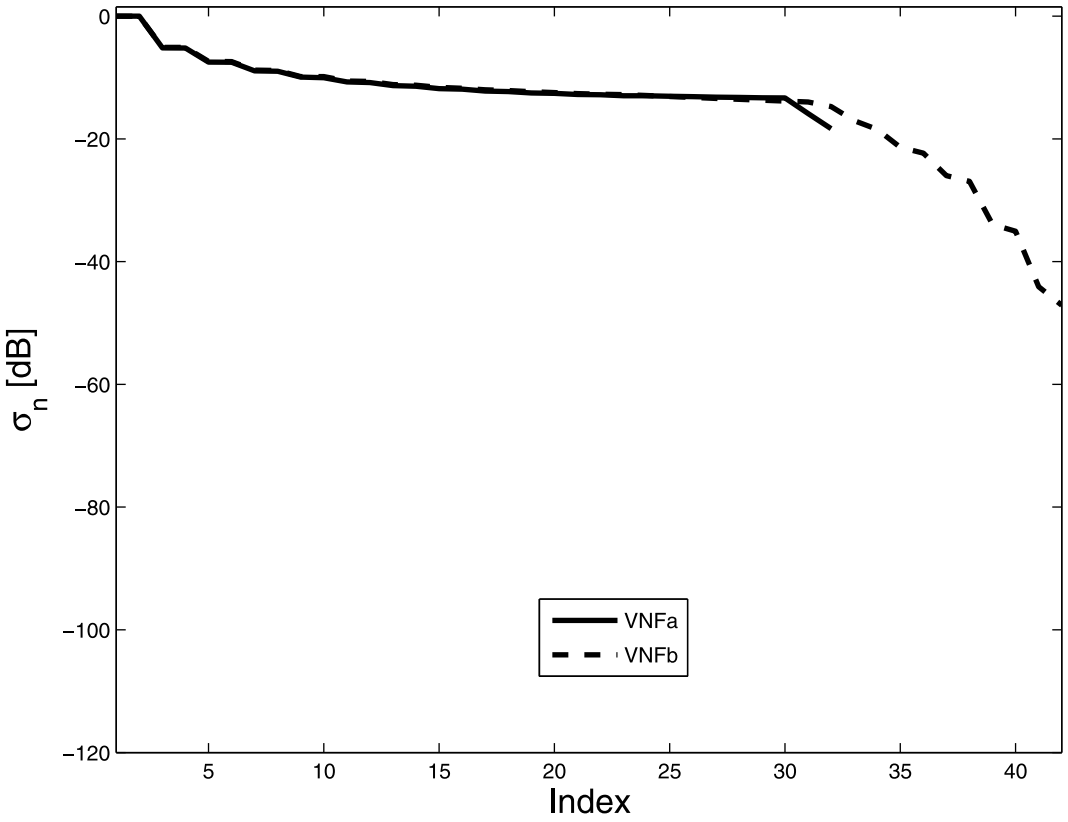

Figure 21. Singular values behavior for VNF measurements.

known phase term $\exp[-j(\beta\sin\alpha)x']$ is included within the kernel of the operator involved in equation (9).

[83] Figure 23 shows the choice of M when $\alpha = 10°$, $a = 15\lambda$, $a' = 7\lambda$, $d = 5\lambda$, $N = 32$. As it can be seen, the expected saturation behavior of the optimal values of Φ is obtained also for this case. On the other side, Figure 24 illustrates the behavior of the singular values corresponding to the saturation value $M = 39$. Figure 25 shows the obtained sampling locations. As it can be seen, the approach is consistent since it is capable to provide the accumulation of the sampling points away from the z axis, i.e., when the field is expected to be significant due to the phase tilt on J. Finally, Figure 26 illustrates the reconstruction of the exponentially tapered source with noisy measurements and SNR = 30dB. The obtained root mean square errors have been 3.62% and 7.64% for the proposed procedure and the sampling performed according to *Bucci and D'Elia* [1996] and *Bucci et al.* [1998], respectively.

[84] Let us now deal with flexibility. It is worth finally mentioning that the proposed approach is able to deal with arbitrarily shaped measurement domains. For example, elliptic domains have been considered, but are not reported. We here illustrate the case of an acquisition domain formed by a piecewise linear (i.e., nonanalytical) curve D_I [*Gregson et al.*, 2003] which cannot be managed by the approach by *Bucci and D'Elia* [1996] and *Bucci et al.* [1998]. Figures 23, 24, and 27 illustrate the obtained results thereof. As for section 6.1, also for the present one, a uniform sampling has been considered as starting point for the optimization of Φ.

6.4. Sources With Circular Support

[85] In this section, we briefly illustrate the case when the domain D_S is a circle, centered at the origin of the $Oxyz$ reference system, of radius ρ_c so that ∂D_S is a circumference. For the sake of brevity, we deal again with a 2-D scalar source ($\underline{J} = J\hat{i}_y$) and we focus the attention to the selection of the sampling points on D_I only.

[86] The relevant Green's function can be expressed as

$$G(\underline{\rho}, \underline{\rho}') = \frac{\beta^2}{4\omega\varepsilon} \sum_{n=-\infty}^{+\infty} \frac{H_n^{(2)}(\beta\rho_c) J_n'(\beta\rho_c)}{H_n^{(2)'}(\beta\rho_c)} \cdot H_n^{(2)}(\beta\rho) e^{jn(\varphi-\varphi')}, \tag{12}$$

where J_n and J_n' are the Bessel function of nth order and its derivative, respectively, $H_0^{(2)}$ and $H_0^{(2)\prime}$ are the

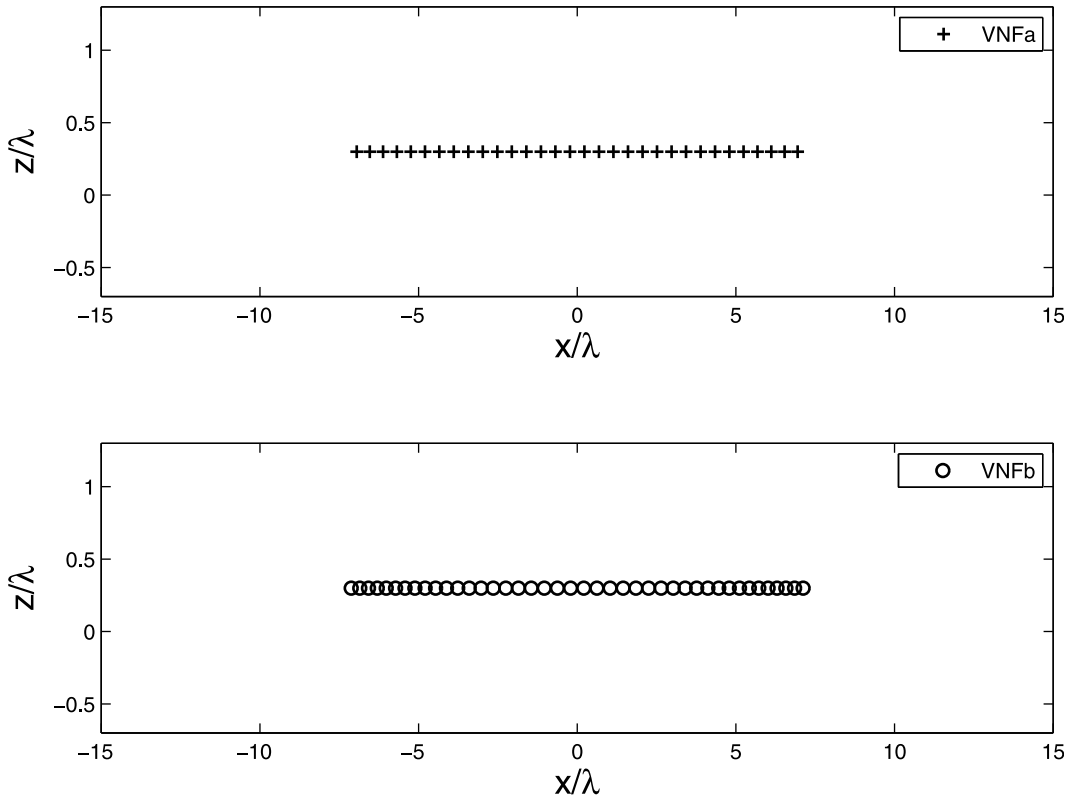

Figure 22. Sampling point locations for VNF measurements.

Hankel function of nth order and second kind and its derivative, respectively, $\underline{\rho} = (\rho\cos\varphi,\rho\sin\varphi)$ and $\underline{\rho}' = (\rho_c\cos\varphi',\rho_c\sin\varphi')$.

[87] For the case at hand, it is convenient to represent J as

$$J(\varphi') = \sum_{n=0}^{N-1} I_n e^{jk\varphi'}, \tag{13}$$

Figure 28 illustrates the sampling points obtained when $\rho_c = 4\lambda$, $D_I = (-a,a)$, $a = 40\lambda$, $d = 6\lambda$. The number of selected sampling points has resulted to be $M = 46$.

7. Extension to the Scalar 3-D Case

[88] In this section, we provide an extension of the approach to the scalar ($\underline{J} = J\hat{i}_y$), 3-D case for rectangular, parallel domains. Once again, $D_I = D_O$ and the operators $\mathcal{A}_I$ and $\mathcal{A}_O$ can be expressed as:

$$E(x,y)\hat{i}_y = \mathcal{A}_I\left(J\hat{i}_y\right) = \mathcal{A}_O\left(J\hat{i}_y\right) = -j\omega\mu \int_{-a'}^{a'} \int_{-b'}^{b'} J(x',y')\hat{i}_y \frac{e^{-j\beta R}}{4\pi R} dx'dy', \tag{14}$$

where $R = \sqrt{(x-x')^2 + (y-y')^2 + d^2}$, the rectangle $(-a', a') \times (-b', b')$ of the $z = 0$ plane is the source support, the rectangle $(-a, a) \times (-b,b)$ of the $z = d$ plane is the domain $D_I = D_O$.

[89] The same above discussed guidelines (section 4.3) concerning the choice of the basis functions to expand $\underline{J}$ and on the discretization of the involved operators apply also in this case. Likewise, the determination of the "optimal" samples number and locations are performed by the optimization of functional Φ (see section 4.2).

[90] Concerning the computational complexity, on assuming that N is the overall number of basis functions employed to expand the current distribution, that P is the number of measured vector components of the field and that M is the number of sampling points, then $\underline{\underline{Z}}$ is once again a $PM \times N$ matrix. Accordingly, the burden for evaluating the full SVD of $\underline{\underline{Z}}$ (needed to solve the $\underline{V} = \underline{\underline{Z}}\,\underline{I}$ system) or for its singular values only (needed for evaluating the functional Φ) can be estimated with the same formulas as for the 2-D case. Obviously, the typical values of N and M involved in the 3-D case will be larger than those concerning the 2-D one, leading to a generally higher computational cost.

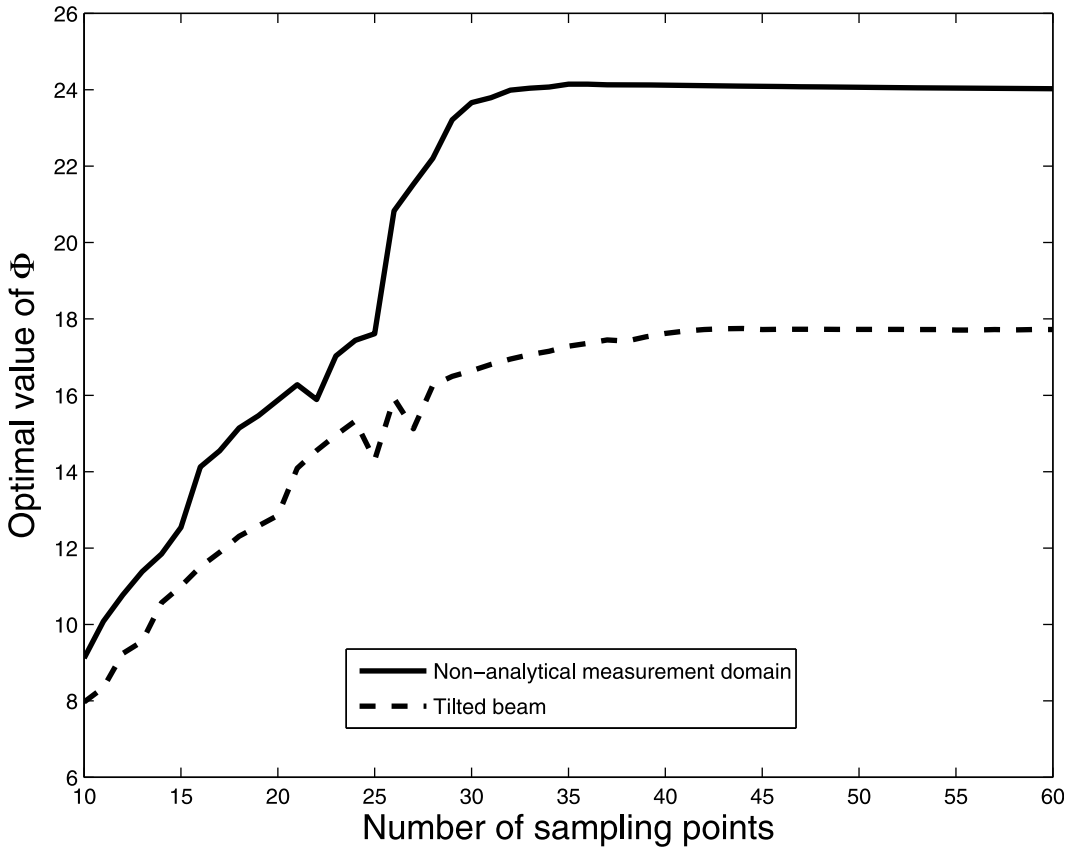

Figure 23. Illustration of the choice of M for the cases of a tilted beam and of a nonanalytical measurement domain.

[91] For this case, equation (7) turns into [*Capozzoli et al.*, 2009a]

$$J(x',y') = \sum_{n,m} J_{nm}\Phi_n[c_x,x']\Phi_m[c_y,y'] \qquad (15)$$

where $c_x = \beta a$' and $c_y = \beta b$', to represent J.

[92] Furthermore, also in this case, it is possible to provide a proper representation of the sampling points to limit the number of parameters to be determined while optimizing Φ. Indeed, the $z = d$ plane can be regarded as a Riemannian manifold with admissible representation [*Bishop and Goldberg*, 1980]

$$(x,y) = (h(\xi,\eta), l(\xi,\eta)), \qquad (16)$$

where the functions h and l are expanded as

$$\begin{cases} h(\xi,\eta) = \sum_{r=1}^{R}\sum_{s=1}^{S} \alpha_{rs} L_r(\xi) L_s(\eta) \\ g(\xi,\eta) = \sum_{r=1}^{R}\sum_{s=1}^{S} \beta_{rs} L_r(\xi) L_s(\eta) \end{cases}, \qquad (17)$$

in which the L_k's are properly chosen (e.g., polynomial) expansion functions (see section 6.1) and α_{rs} and β_{rs} are the corresponding expansion coefficients to be determined. Following (16) and (17), the sampling points are represented as

$$(x_m,y_m) = (h(\xi_m,\eta_m), l(\xi_m,\eta_m)), \qquad (18)$$

where (ξ_m, η_m) is a uniformly sampled grid in $(-1,1) \times (-1,1)$. In the numerical example below, the functions L_k are chosen, as done before, as Legendre polynomials.

[93] Figure 29 depicts the obtained sampling points locations for the case when $a' = b' = 3\lambda$, $a = b = 7\lambda$ and $d = 5\lambda$. The overall number of sampling points has resulted equal to $M = 169$.

8. Conclusions and Future Developments

[94] The problem of extracting the maximum amount of information on an electromagnetic field over a domain D_O from field sample measurements on a domain D_I,

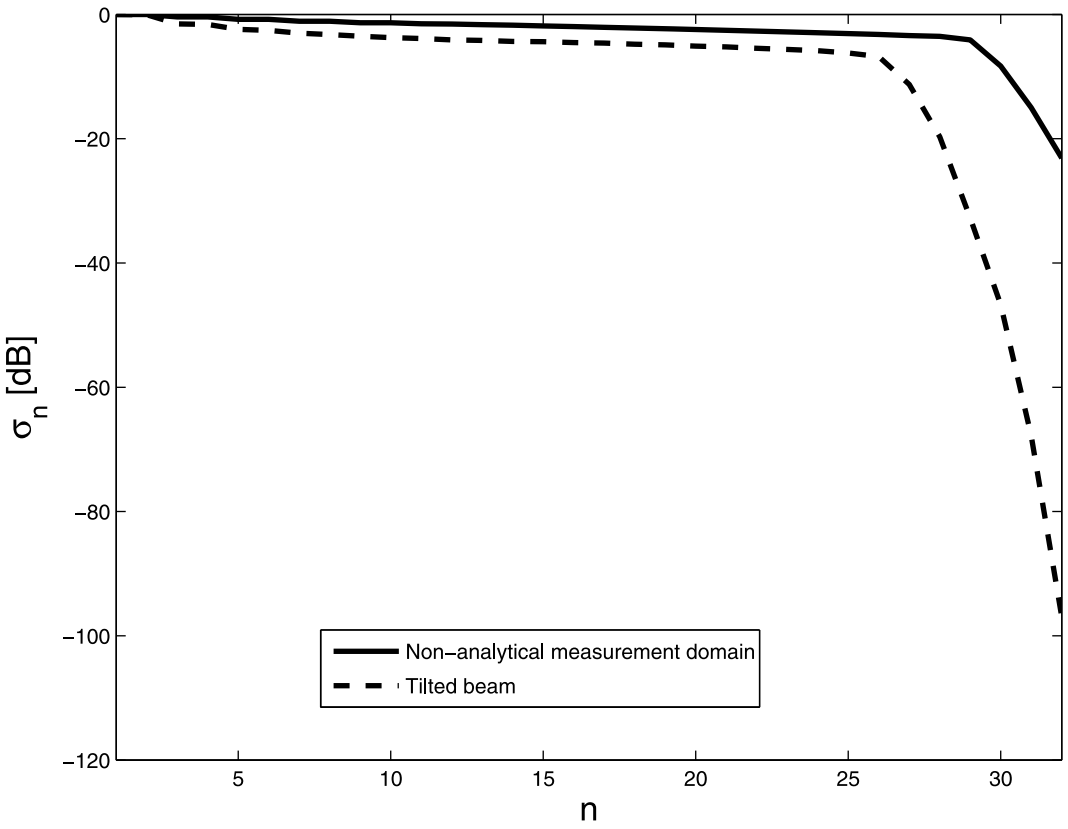

Figure 24. Singular values behavior for the case of a tilted beam and of a nonanalytical measurement domain.

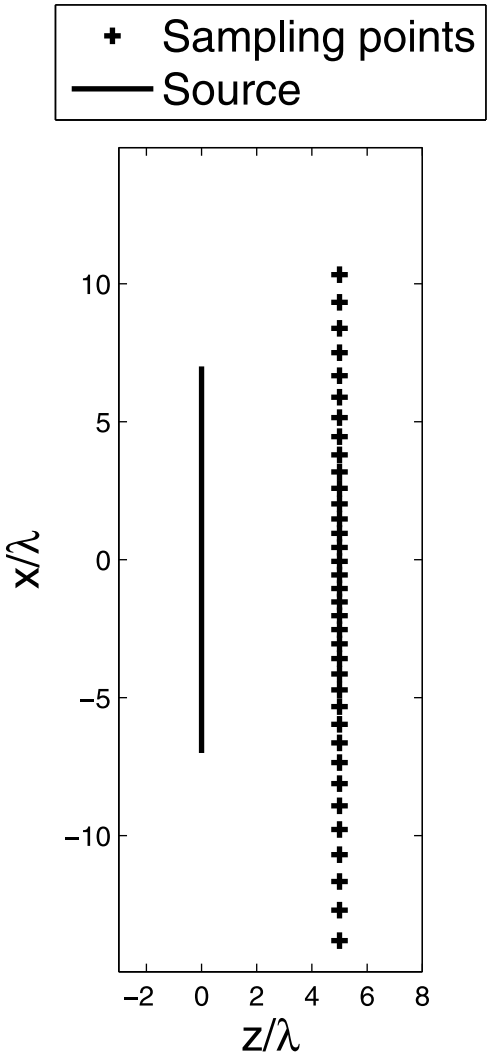

Figure 25. Sampling locations for the case of a tilted beam.

with a priori information on the source (or scatterer) has been dealt with. The field sample locations maximizing the amount of information extracted from D_I to accurately determining the field on D_O have been chosen according to a singular values optimization procedure. An extensive numerical analysis has highlighted the better performance, consistency and flexibility of the approach as compared to another already available approach which, till now, has been proven to be successful in the applications. Furthermore, it has been shown that the approach allows performing acquisitions in the VNF or on arbitrarily shaped (and in particular nonanalytical) domains D_I and to deal with electrically small sources or with radiating tilted beams.

[95] We remark that the approach is capable to significantly reducing the number of the required field samples as compared to the brutal, and widely used, $\lambda/2$ uniform sampling. This strongly reduces the measurement time, especially for electrically large antennas. Such a reduction requires a computational effort, though, related to the repeated evaluation of the singular values at each step of an iterative procedure. Nevertheless, the number of iterations can be reduced by a careful choice of the starting guess (e.g., according to *Bucci and D'Elia* [1996] and *Bucci et al.* [1998]). Furthernore, any solution lowering the value of the functional Φ as compared to the starting point leads to an improved solution thereof.

[96] As future developments, let us stress that the approach can be further strengthened against the local minima problem by aid of global techniques for the optimization of the functional Φ [*Capozzoli and D'Elia*, 2006] (see also *Horst and Tuy* [1990] and *van Laarhoven and Aarts* [1988], *Bäck et al.* [1997], *Weile and Michielssen* [1997], *Caorsi et al.* [2000], *Qing* [2003], *Robinson and Rahmat-Samii* [2004], *Donelli and Massa* [2005], and *Massa et al.* [2005] for references concerning deterministic and stochastic algorithms, respectively, or *Capozzoli et al.* [2007] for a multistage approach).

[97] It can be generalized to higher dimensions (including volumetric sampling and frequency dependences of the source), by optimizing the field polarization too, and eventually to the case of inhomogeneous backgrounds.

[98] The approach can be exploited also in the case of static fields, in the case of a partially coherent radiation (profiting of the information about the degree of coherence of the signals) or when a more sophisticated statistical modeling of the system and of the noise is available.

[99] Furthermore, the technique can be fruitfully exploited also if the physics of the problem is different from electromagnetism, e.g., in acoustics. More generally, we expect it could be successfully exploited by numerical methods solving, for instance, partial differential equations, wherein the choice of the mesh is often quite troublesome.

[100] Finally, as a further significant application, we mention its connection with information theory [*Gruber and Marengo*, 2008], as is of interest in MIMO systems [*Capozzoli et al.*, 2007], wherein the amount of extracted information could be maximized taking into account the statistics of the involved measurement uncertainties and the degree of coherency of the source [*Wolf*, 1986; *Xu and Janaswamy*, 2006].

Appendix A

[101] The aim of Appendix A is to show how one passes from the closed surface Γ of Figure 1 to the strip in Figure 2. To this end, let us consider the geometry

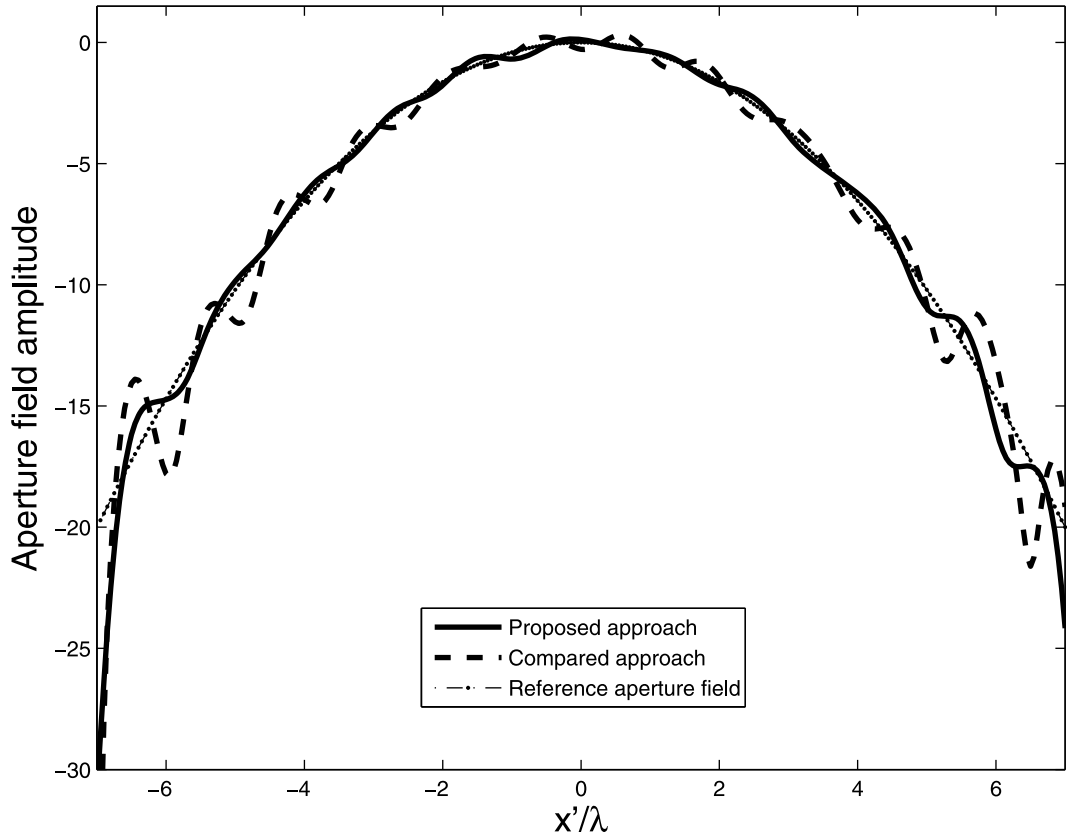

Figure 26. Reconstruction of the exponentially tapered source for the case of a tilted beam.

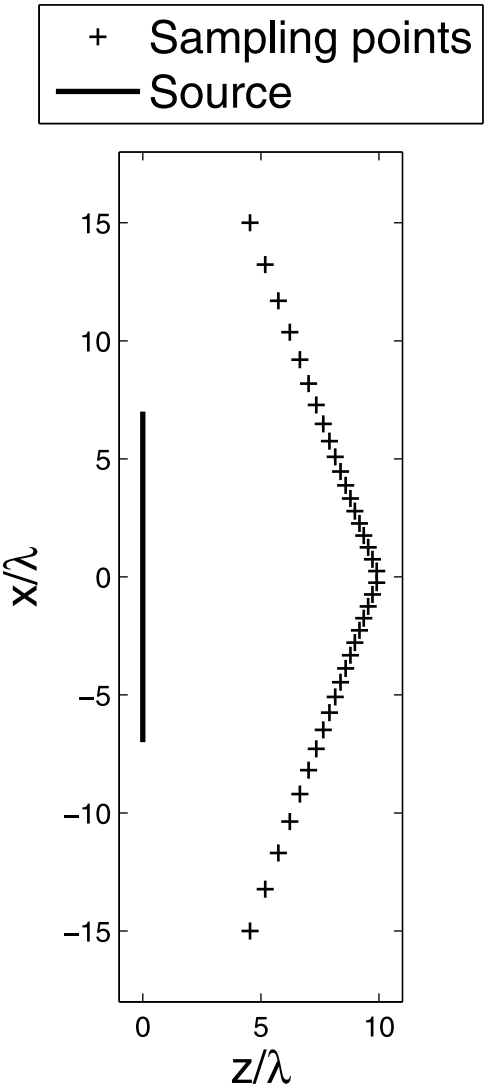

Figure 27. Sampling locations for the case of a nonanalytical measurement domain.

illustrated in Figure A1, in which a planar aperture antenna is embedded within a volume V_a whose contour is composed by a flat surface S_1 (set an infinitesimal distance δ apart from the aperture) and a semisphere S_2 having radius r. Let us also assume that the medium surrounding the antenna is homogeneous, spatially nondispersive and isotropic and define equivalent surface electric and magnetic current densities $\underline{J}_S$ and $\underline{J}_{mS}$ as

$$\begin{cases} \underline{J}_S = \hat{n} \times \underline{H} \\ \underline{J}_{mS} = -\hat{n} \times \underline{E} \end{cases} \tag{A1}$$

defined on S_1 and S_2, where $\hat{n}$ is the unit normal vector outgoing V_a. Application of the reciprocity theorem allows to evaluate the field $\underline{E}_s$ radiated by the surface currents at a point $\underline{r}_0$ in the half-space $z > 0$ as

$$\underline{E}_s(\underline{r}_0) = \iint_{S_1 \cup S_2} (\underline{E} \times \underline{H}_d - \underline{E}_d \times \underline{H}) \cdot \hat{i}_r dS, \tag{A2}$$

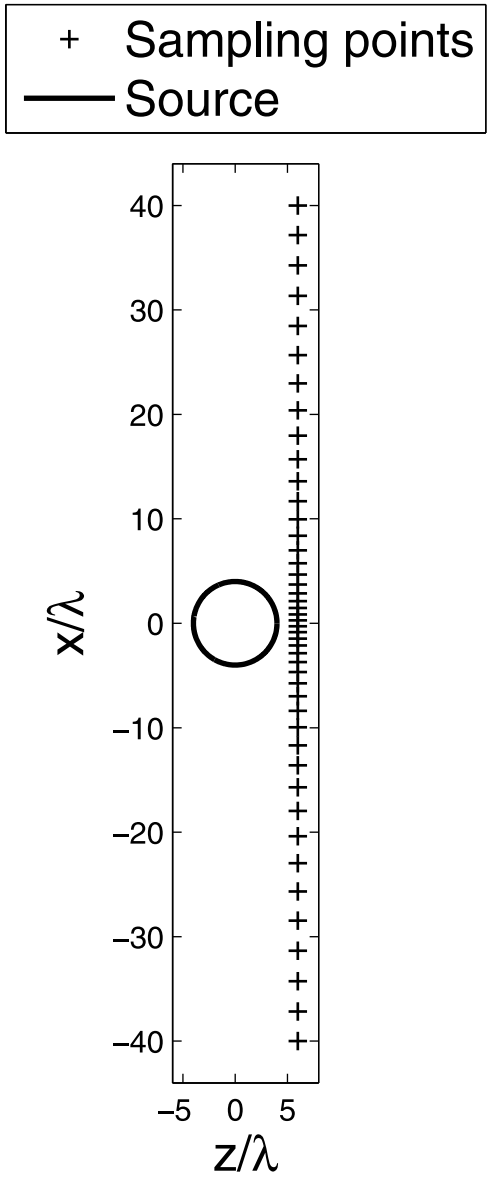

Figure 28. Sampling locations for the case of a source with circular support.

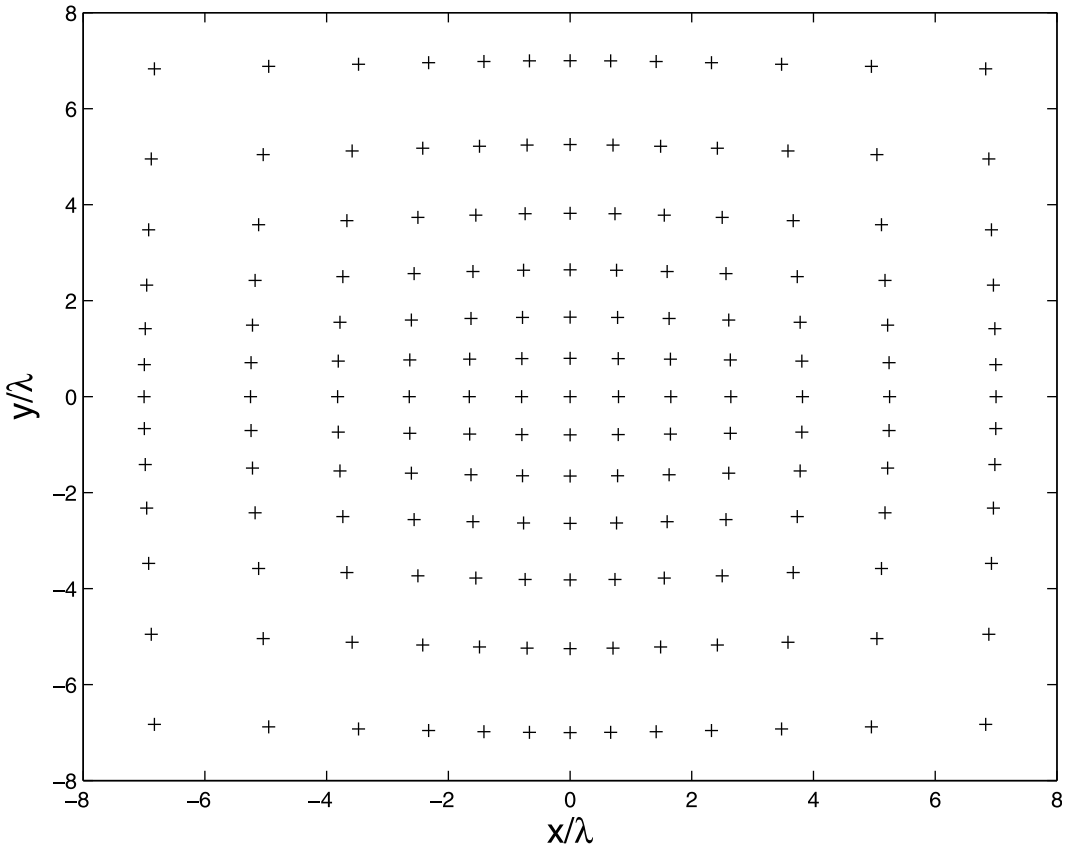

Figure 29. Sampling locations for the scalar, 3-D case.

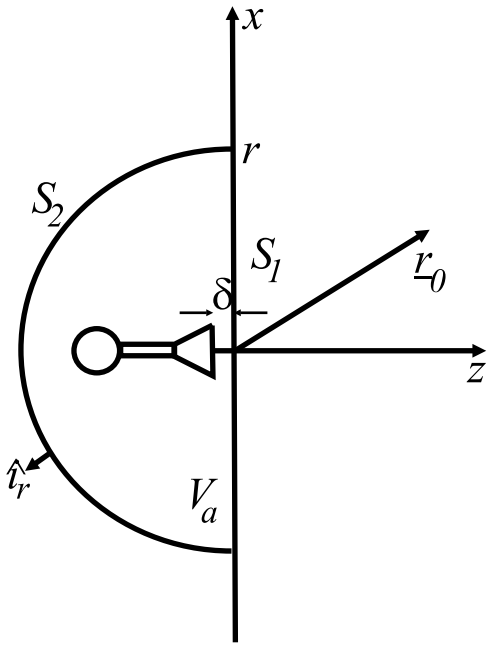

Figure A1. Illustration of the use of the equivalence theorem to evaluate the field radiated by an aperture.

where $\underline{E}$ and $\underline{H}$ are the electric and magnetic field, respectively, produced by the radiator in V_a, and $\underline{E}_d$ and $\underline{H}_d$ are the fields radiated by a dipole located at $\underline{r}$. Due to the Sommerfeld radiation conditions, each contribution due to an elementary surface element dS_2, i.e.,

$$\begin{aligned} \underline{E} &= \zeta \underline{H} \times \hat{i}_r + \underline{o}\left(\frac{1}{r}\right) \\ \underline{E}_d &= \zeta \underline{H}_d \times \hat{i}_r + \underline{o}\left(\frac{1}{r}\right) \end{aligned}, \tag{A3}$$

where ζ is the intrinsic impedance of the medium. Accordingly

$$\lim_{r \to +\infty} \iint_{S_2} (\underline{E} \times \underline{H}_d - \underline{E}_d \times \underline{H}) \cdot \hat{i}_r dS_2 = 0. \tag{A4}$$

[102] In other words, since the integrand is infinitesimal of order larger than two in r, the contribution of the equivalent currents from each portion of the spherical surface S_2, and from the whole S_2, is vanishing for $r \to \infty$. By finally filling V_a with a magnetic perfect conductor, by image theory, the magnetic surface current density does not contribute to $\underline{E}_s(\underline{r}_0)$, while the metal filling can be removed by doubling the electric surface current density on S_1, which is significantly different from zero only across the antenna aperture.

References

Adams, R. A., and J. J. F. Fournier (2003), *Sobolev Spaces*, Elsevier, Oxford, U. K.

Alonso, A. A., C. E. Frouzakis, and I. G. Kevrekidis (2004), Optimal sensor placement for state reconstruction of distributed process systems, *AIChE J.*, *50*(7), 1438–1452.

Ameya, M., P. Vinetti, M. Hirose, S. Kurokawa, G. D'Elia, A. Capozzoli, A. Liseno, and C. Curcio (2009), Phaseless near-field antenna measurement using prolate spheroidal wave functions, in *Proceedings of the IEICE on Advanced Testing and Certification Technology for Radio Equipment* (in Japanese), Inst. of Electron., Inf., and Commun. Eng., Tokyo.

Bäck, T., D. B. Fogel, and Z. Michalewicz (1997), *Handbook of Evolutionary Computation*, Inst. of Phys., Bristol, U. K.

Barakat, R. (1964), Application of the sampling theorem to optical diffraction theory, *J. Opt. Soc. Am.*, *54*(7), 920–930.

Bertero, M., and C. De Mol (1996), Super-resolution by data inversion, in *Progress in Optics*, vol. 36, edited by E. Wolf, pp. 129–178, Elsevier, Amsterdam.

Bertero, M., C. De Mol, and G. A. Viano (1979), On the problems of object restoration and image extrapolation in optics, *J. Math Phys.*, *20*(3), 509–521.

Bishop, R. L., and S. I. Goldberg (1980), Tensor Analysis on Manifolds, Dover, Mineola, N. Y.

Bleistein, N., and J. K. Cohen (1977), Nonuniqueness in the inverse source problem in acoustics and electromagnetics, *J. Math Phys.*, *18*(2), 194–201.

Bucci, O. M., and G. D'Elia (1996), Advanced sampling techniques in electromagnetics, in *Review of Radio Science 1993–1996*, pp. 177–204, Oxford Univ. Press, London.

Bucci, O. M., and G. Di Massa (1988), The truncation error in the application of sampling series to electromagnetic problems, *IEEE Trans. Antennas Propag.*, *36*(7), 941–949.

Bucci, O. M., C. Gennarelli, and C. Savarese (1998), Representation of electromagnetic fields over arbitrary surfaces by a finite and nonredundant number of samples, *IEEE Trans. Antennas Propag.*, *46*(3), 351–359.

Caorsi, S., A. Massa, and M. Pastorino (2000), A computational technique based on a real-coded genetic algorithm for microwave imaging purposes, *IEEE Trans. Geosci. Remote Sens.*, *38*(4), 1697–1708.

Capozzoli, A., and G. D'Elia (2006), Global optimization and antennas synthesis and diagnosis, part one: Concepts, tools, strategies and performances, *Prog. Electromagn. Res.*, *56*, 195–232.

Capozzoli, A., C. Curcio, G. D'Elia, and A. Liseno (2007), Power pattern synthesis of multifeed reconfigurable reflectarrays, in *Proceedings of the 29th ESA Antenna Workshop on Multiple Beams Reconfigurable Antennas* [CD ROM], Eur. Space Agency, Noordwijk, Netherlands.

Capozzoli, A., C. Curcio, G. D'Elia, A. Liseno, and P. Vinetti (2008), FFT and equivalently tapered aperiodic arrays, in *Proceedings of the XXIX URSI General Assembly* [CD ROM], Int. Union of Radio Sci., Chicago, Ill.

Capozzoli, A., C. Curcio, G. D'Elia, and A. Liseno (2009a), Phaseless antenna characterization by effective aperture field and data representations, *IEEE Trans. Antennas Propag.*, *57*(1), 215–230.

Capozzoli, A., C. Curcio, G. D'Elia, A. Liseno, P. Vinetti, M. Ameya, M. Hirose, S. Kurokawa, and K. Komiyama (2009b), Dielectric field probes for very-near-field and compact-near-field antenna characterization, *IEEE Antennas Propag. Mag.*, *51*(5), 118–125.

Capozzoli, A., C. Curcio, G. D'Elia, A. Liseno, and P. Vinetti (2009c), A novel approach to the design of generalized plane-wave synthesizers, in *Proceedings of the 3rd European Conference on Antennas and Propagation* [CD ROM], Berlin, Germany.

Cathey, W. T., B. R. Frieden, W. T. Rhodes, and C. K. Rushforth (1984), Image gathering and processing for enhanced resolution, *J. Opt. Soc. Am. A*, *1*(3), 241–250.

Chan, T. F., J. Shen, and L. Vese (2003), Variational PDE models in image processing, *Notices*, *50*(1), 14–26.

Chew, W. C., Y. M. Wang, G. Otto, D. Lesselier, and J. C. Bolomey (1994), On the inverse source method of solving inverse scattering problems, *Inverse Probl.*, *10*(3), 547–553.

Clark, J. J., M. R. Palmer, and P. D. Lawrence (1985), A transformation method for the reconstruction of functions from nonuniformly spaced samples, *IEEE Trans. Acoust. Speech Signal Process.*, *33*(4), 1151–1165.

Collin, R. E. (1991), *Field Theory of Guided Waves*, IEEE Press, New York.

Courjon, D. (2003), *Near-Field Microscopy and Near-Field Optics*, Imperial College Press, London.

Curtis, A. (2002), Optimal experiment design: Cross-borehole tomographic examples, *Geophys. J. Int.*, *136*(3), 637–650.

D'Elia, G., G. Leone, R. Pierri, and G. Schirinzi (1985), 'Traveling' sampling of scattered fields, *Proc. Antennas Propag. Int. Symp.*, *23*, 531–534.

Derat, B., A. Cozza, and J. C. Bolomey (2007), Influence of source-phantom multiple interactions on the field transmitted in a flat phantom, in *Proceedings of the International Symposium on Electromagnetic Compatibility*, pp. 139–142, Inst. of Electr. and Electron. Eng., Zurich, Switzerland.

Devaney, A. J. (2004), Nonradiating surface sources, *J. Opt. Soc. Am. A Opt. Image Sci. Vis.*, *21*(11), 2216–2222.

Devaney, A. J., and E. A. Marengo (1998), A method for specifying non-radiating, monochromatic, scalar sources and their fields, *Pure Appl. Opt.*, *7*(5), 1213–1220.

Devaney, A. J., and E. Wolf (1973), Radiating and nonradiating classical current distributions and the fields they generate, *Phys. Rev. D*, *8*(4), 1044–1047.

De Villiers, G. D., F. B. T. Marchaud, and E. R. Pike (2001), Generalized Gaussian quadrature applied to an inverse problem in antenna theory, *Inverse Probl.*, *17*(4), 1163–1179.

Donelli, M., and A. Massa (2005), Computational approach based on a particle swarm optimizer for microwave imaging of two-dimensional dielectric scatterers, *IEEE Trans. Microwave Theory Tech.*, *53*(5), 1761–1776.

Fernando, V. K., and B. N. Parlett (1994), Accurate singular values and differential qd algorithms, *Numer. Math.*, *67*(2), 191–229.

Fok, F. Y. S., and J. D. Young (1987), Space-frequency sampling criteria for electromagnetic scattering of a finite object, *IEEE Trans. Antennas Propag.*, *35*(8), 920–925.

Golub, G. H., and C. F. Van Loan (1996), *Matrix Computations*, John Hopkins Univ. Press, Baltimore, Md.

Gori, F., and G. Guattari (1973), Shannon number and degrees of freedom of an image, *Opt. Commun.*, *7*(2), 163–165.

Gregson, S. F., C. G. Parini, and J. McCormick (2003), Wide angle antenna pattern measurements using a poly planar near field technique, in *Proceedings of the 12th International Conference on Antennas and Propagation.*, pp. 111–114, Univ. of Exeter, Exeter, U. K.

Gruber, F. K., and E. A. Marengo (2008), New aspects of electromagnetic information theory for wireless and antenna systems, *IEEE Trans. Antennas Propag.*, *56*(11), 3470–3484.

Horst, R., and H. Tuy (1990), *Global Optimization: Deterministic Approaches*, Springer, Berlin.

Jones, D. S. J. (1995), *Methods in Electromagnetic Wave Propagation*, IEEE Press, New York.

Kao, C. M., X. Pan, P. La Riviere, and M. A. Anastasio (1999), Fourier-based optimal recovery method for antialiasing interpolation, *Opt. Eng.*, *38*(12), 2041–2044.

Landau, H. J., and H. O. Pollak (1962), Prolate spheroidal wave functions, Fourier analysis and uncertainty-III: The dimension of essentially time- and band-limited signals, *Bell Syst. Tech. J.*, *41*, 1295–1336.

Langenberg, K. J. (2002), Linear scalar inverse scattering, in *Scattering: Scattering and Inverse Scattering in Pure and Applied Sciences*, edited by R. Pike and P. Sabatier, Academic, London, U. K.

Lewis, A. S. (2003), The mathematics of eigenvalue optimization, *Math. Program., Ser. B*, *97*(1–2), 155–176.

Li, M., A. Abubakar, and P. M. van den Berg (2009), Application of the multiplicative regularized contrast source inversion method on 3D experimental Fresnel data, *Inverse Probl.*, *25*(2), 1–23.

Marks, R. J., II (1980), Coherent optical extrapolation of 2-D band limited signals: Processor theory, *Appl. Opt.*, *19*(10), 1670–1672.

Massa, A., D. Franceschini, G. Franceschini, M. Pastorino, M. Raffetto, and M. Donelli (2005), Parallel GA-based approach for microwave imaging applications, *IEEE Trans. Antennas Propag.*, *53*(10), 3118–3127.

McWhirter, J. G., and E. R. Pike (1978), On the numerical inversion of the Laplace transform and similar Fredholm integral equations of the first kind, *J. Phys. A Math. Gen.*, *11*(9), 1729–1745. (Available at http://www.netlib.org/lapack/lug/node53.html)

Paris, D., W. Leach, and E. Joy (1978), Basic theory of probe-compensated near-field measurements, *IEEE Trans. Antennas Propag.*, *26*(3), 373–379.

Pierri, R., and F. Soldovieri (1998), On the information content of the radiated fields in the near zone over bounded domains, *Inverse Probl.*, *14*(2), 321–337.

Pierri, R., G. D'Elia, and F. Soldovieri (1999), A two probes scanning phaseless near-field far-field transformation technique, *IEEE Trans. Antennas Propag.*, *47*(5), 792–802.

Piestun, R., and D. A. B. Miller (2000), Electromagnetic degrees of freedom of an optical system, *J. Opt. Soc. Am. A Opt. Image Sci. Vis.*, *17*(5), 892–902.

Pike, E. R., J. G. McWhirter, M. Bertero, and C. de Mol (1984), Generalized information theory for inverse problems in signal processing, *IEE Proc., Part F*, *131*(6), 660–667.

Qing, A. (2003), Electromagnetic inverse scattering of multiple two-dimensional perfectly conducting objects by the differential evolution strategy, *IEEE Trans. Antennas Propag.*, *51*(6), 1251–1262.

Rahmat-Samii, Y., V. Galindo-Israel, and R. Mittra (1980), A plane-polar approach for far-field construction from near-field measurements, *IEEE Trans. Antennas Propag.*, *28*(2), 216–230.

Robinson, J., and Y. Rahmat-Samii (2004), Particle swarm optimization in electromagnetics, *IEEE Trans. Antennas Propag.*, *52*(2), 397–407.

Salerno, E. (1998), Generalized prolate spheroidal wavefunctions associated to a particular space-limited 2D band-pass operator, *CNR Rep.*, *|E|:B4–31–10–1998.*

Schreier, H. W., J. R. Braasch, and M. A. Sutton (2000), Systematic errors in digital image correlation caused by intensity interpolation, *Opt. Eng.*, *39*(11), 2915–2921.

Severcan, M. (1982), Restoration of images of finite extent objects by a singular value decomposition technique, *Appl. Opt.*, *21*(6), 1073–1076.

Sten, J. C. E. (2004), Reconstruction of electromagnetic minimum energy sources in a prolate spheroid, *Radio Sci.*, *39*, RS2020, doi:10.1029/2003RS002973.

Sten, J. C. E., and E. A. Marengo (2006), Inverse source problem in an oblate spheroidal geometry, *IEEE Trans. Antennas Propag.*, *54*(11), 3418–3428.

Sten, J. C. E., and E. A. Marengo (2008), Inverse source problem in the spheroidal geometry: Vector formulation, *IEEE Trans. Antennas Propag.*, *56*(4), 961–969.

Tai, C. T. (1993), *Dyadic Green Functions in Electromagnetic Theory*, IEEE Press, New York.

Toraldo di Francia, G. (1952), Super-gain antennas and optical resolving power, *Nuovo Cim.*, *9*, suppl. 3, 426–438.

Toraldo di Francia, G. (1955), Resolving power and information, *J. Opt. Soc. Am.*, *45*(7), 497–501.

Tuy, H. (1998), *Convex Analysis and Global Optimization*, Kluwer Acad., Dordrecht, Netherlands.

Twomey, S. (1965), The application of numerical filtering to the solution of integral equations encountered in indirect sensing measurements, *J. Franklin Inst.*, *279*, 95–109.

van Laarhoven, P. J., and E. H. Aarts (1988), *Simulated Annealing: Theory and Applications*, Kluwer Acad., Dordrecht, Netherlands.

Vinetti, P. (2008), A non-invasive, near-field and very near-field phaseless antenna characterization system, Ph.D. thesis, Univ. di Napoli Federico II, Naples, Italy. (Available at http://www.fedoa.unina.it/3499/1/Tesi_Dottorato_vinetti_pietro.pdf)

Weile, D. S., and E. Michielssen (1997), Genetic algorithm optimization: A review, *IEEE Trans. Antennas Propag.*, *45*(3), 343–353.

Wolf, E. (1986), New theory of partial coherence in the space-frequency domain. Part II: Steady-state fields and higher-order correlations, *J. Opt. Soc. Am. A*, *3*(1), 76–85.

Xu, J., and R. Janaswamy (2006), Electromagnetic degrees of freedom in 2D scattering environments, *IEEE Trans. Antennas Propag.*, *54*(12), 3882–3894.

Yaghjian, A. (1986), An overview of near-field antenna measurements, *IEEE Trans. Antennas Propag.*, *34*(1), 30–45.

Zeevi, Y. Y., and E. Shlomot (1993), Nonuniform sampling and antialiasing in image representation, *IEEE Trans. Acoust. Speech Signal Process.*, *41*(3), 1223–1236.

A. Capozzoli, C. Curcio, A. Liseno, and P. Vinetti, Dipartimento di Ingegneria Biomedica, Elettronica e delle Telecomunicazioni, Università di Napoli Federico II, via Claudio 21, I-80125 Napoli, Italy. (a.capozzoli@unina.it)